

## The Orion Molecular Cloud 2/3 and NGC 1977 Regions

Dawn E. Peterson

*Harvard-Smithsonian Center for Astrophysics*  
*60 Garden Street, Cambridge, MA 02138, USA*

S. Thomas Megeath

*Ritter Observatory MS 113, University of Toledo*  
*2801 W. Bancroft St, Toledo, OH 43606, USA*

**Abstract.** The Orion Molecular Cloud 2/3 region (hereafter, OMC-2/3) and the reflection nebula NGC 1977 encompass a section of the Orion A molecular cloud undergoing vigorous star forming activity. One of the richest assemblages of protostars in the nearest 500 pc is seen in OMC-2/3, while NGC 1977 contains a cluster of over 100 young stars. In this review, we present a census of the protostars, pre-main sequence stars, and young brown dwarfs in these regions. These are identified through sub-millimeter surveys, far-red to near-infrared imaging and spectroscopy with ground-based telescopes, mid-infrared photometry from the *Spitzer Space Telescope*, and X-ray observations made with the Chandra X-ray Observatory. We present an overview of the distribution of molecular gas associated with these regions and the rich complex of shock heated nebulae created by the young stars interacting with the molecular gas. Finally, we discuss the relationship of OMC-2/3 and NGC 1977 to the neighboring Orion Nebula Cluster and the Orion OB1 association.

### 1. Introduction

The section of the Orion A molecular cloud directly north of the Orion Nebula is a region of intense star formation activity. Although the number and density of young stars in this area does not rival those found in the Orion Nebula, it is still one of the most active regions of ongoing star formation within 500 pc of the Sun. It is typically divided into two regions: the Orion Molecular Cloud 2/3 region, which contains a filamentary molecular cloud rapidly forming new stars, and NGC 1977, a composite reflection and emission line nebula. In this chapter, we will review the observations which delineate the stellar, sub-stellar, protostellar and gas content in these two regions. We will begin by discussing the distribution of stars, gas and dust in these two regions and their relationship to the Orion Nebula Cluster.

### 2. The Large Scale Distribution of Stars, Gas and Dust in OMC-2/3 and NGC 1977

The Orion Molecular Cloud 2/3 (hereafter OMC-2/3), NGC 1977 and the Orion Nebula region are part of the Orion OB 1 complex (see Figure 1); these regions fall along the line-of-sight of the Orion 1c (4.6 Myr) and 1d (< 1 Myr) subgroups (Brown, de Geus, & de Zeeuw 1994). There are 15 OB stars in the subgroup 1c and 18 OB stars in subgroup 1d (Goudis 1982). Warren & Hesser (1978) place the Trapezium stars of the Orion Nebula

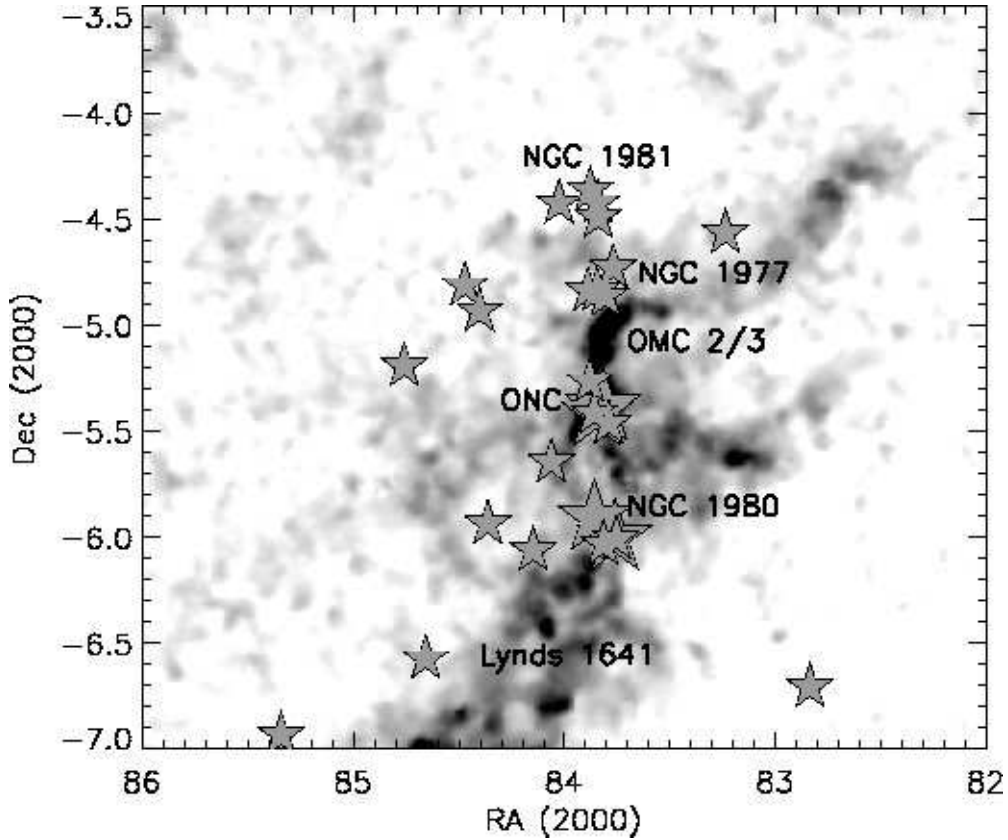


Figure 1. The distribution of OB stars surrounding the OMC-2/3 and NGC 1977 regions. The greyscale image is an extinction map of the Orion A cloud generated from the 2MASS PSC (Gutermuth, private communication). The star shaped markers are the OB stars in the OB 1 association (Brown 1996); the small markers are the B stars and the large markers are the O stars. These show that the OMC-2/3 and NGC 1977 regions are surrounded by a number of B stars, particular to the north of NGC 1977 and the east of OMC-2/3. These OB stars are likely members of the 1c subgroup.

in the Orion 1d association and the most massive star in NGC 1977 in Orion 1c. The division of stars into subgroups has been done primarily by their spatial distribution, yet there may be significant spatial overlap between the subgroups (see, for example, Jeffries et al. (2006)). Thus, the membership of the two subgroups and the relationship of the subgroups to the current star formation in OMC-2/3 is far from clear. Surrounding OMC-2/3 and NGC 1977 are a number of B stars. Directly north of NGC 1977, and outside the molecular cloud, is the NGC 1981 cluster which contains four B stars. To the east of OMC-2/3 are three B stars. The relationship of these stars to the OMC-2/3 and NGC 1977 regions is not understood; it is plausible that they have influenced star formation in these regions by compressing, heating and/or ionizing the molecular gas in the Orion A cloud.

In Figure 2, we show the relationship of OMC-2/3 and NGC 1977 to the Orion Nebula using the positions of known young stars and protostars and maps of the dust

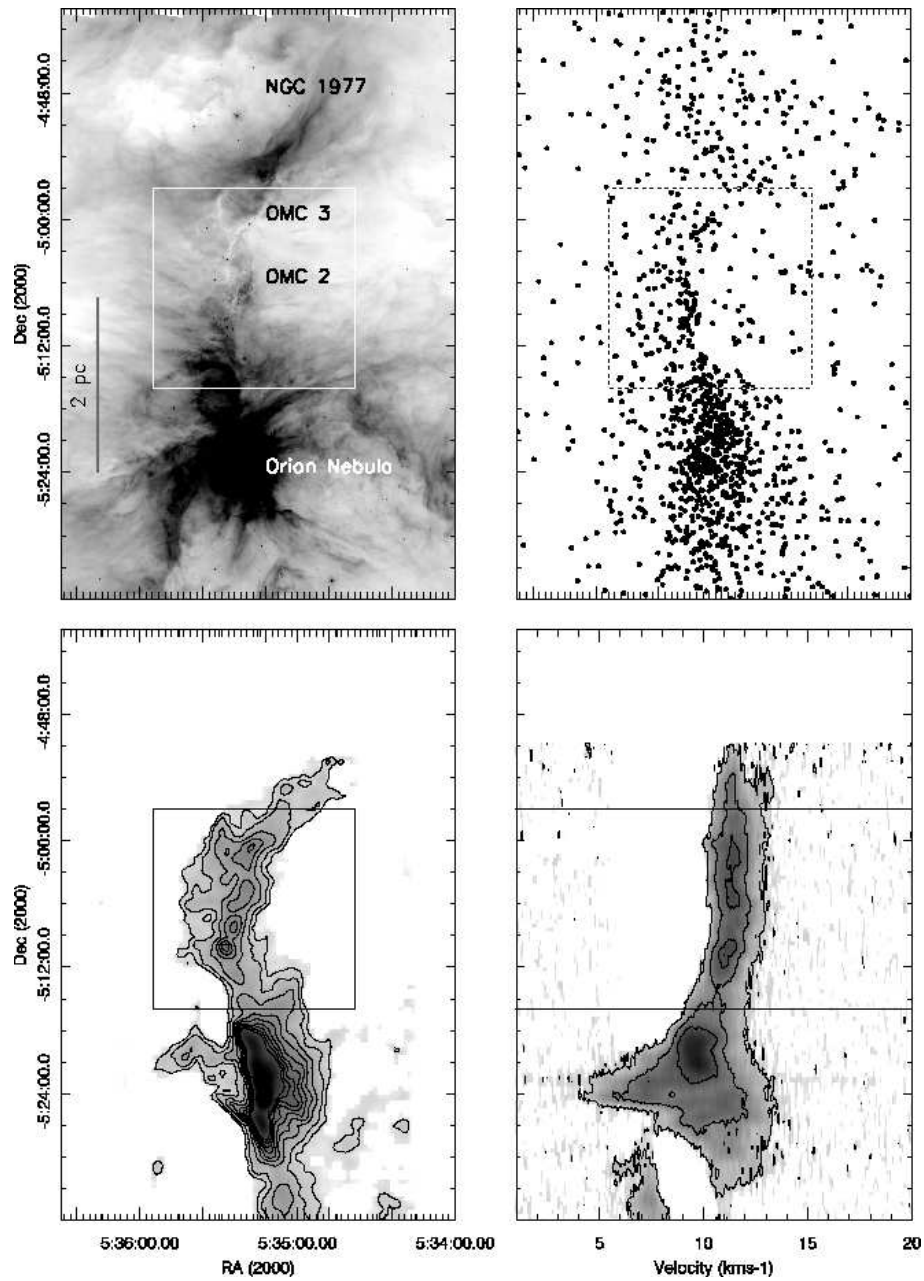


Figure 2. OMC-2/3, NGC 1977, and the Orion Nebula Cluster. The upper left panel shows  $8\ \mu\text{m}$  emission observed with IRAC on *Spitzer*. The box shows the  $20' \times 20'$  field mapped by Peterson et al. (2008). The upper right panel shows the distribution of young stars and protostars identified by variability or infrared excess (Carpenter, Hillenbrand, & Skrutskie 2001; Megeath et al. 2008a, in prep). This map is incomplete toward the center of the Orion Nebula cluster. The lower left panel shows the distribution of velocity integrated CS  $2 \rightarrow 1$  emission mapped by Five College Radio Astronomy Observatory (N. Ridge, priv. comm.). The lower right panel shows a radial velocity versus declination plot of the same data cube integrated over RA. The two lines show the extent of the box shown in the other panels.

and gas emission. The *Spitzer* 8  $\mu\text{m}$  map shows the emission of UV heated small grains and hydrocarbons. The Orion Nebula is the region of bright 8  $\mu\text{m}$  emission in the southern part of the map. Extended diffuse emission is detected in OMC-2/3. Within this emission, dense molecular filaments are apparent in absorption against the diffuse emission. This filamentary cloud of dense molecular gas is seen in the lower angular resolution CS (2  $\rightarrow$  1) map. Apart from a shift in the molecular gas velocity, as shown in the declination-velocity map, the gas in the OMC-2/3 region appears to be a continuation of the same gas associated with the Orion Nebula. NGC 1977 is surrounded by a loop in the 8  $\mu\text{m}$  emission; the emission is brightest where the loop meets the dense molecular gas.

Two studies have identified the pre-main sequence and protostellar sources throughout the entire region displayed in Figure 2. Carpenter, Hillenbrand, & Skrutskie (2001) used multi-epoch  $JHK_S$ -band imaging of a  $0.84^\circ \times 6^\circ$  region centered on the Orion Nebula to examine variability in young stars. Variable stars in this sample are likely to be young pre-main sequence stars. More recently, Megeath et al. (2008a, in prep) have identified infrared excess sources in the Orion A molecular cloud by combining mid-infrared photometry from the *Spitzer* Space Telescope with the Two Micron All Sky Survey (2MASS) point source catalog (Skrutskie et al. 2006); these sources are young pre-main sequence stars and protostars with dusty disks and envelopes.

The observations show a continuous distribution of young stars extending from the Orion Nebula, where the density of young stars is highest, out to the NGC 1977 region. The region of peak density is often referred to as the Orion Nebula Cluster (hereafter, ONC, see the chapters by Muench et al. and O'Dell et al.). From the distribution of gas and stars, it is not clear where the ONC ends. Hillenbrand & Hartmann (1998) set an outer radius of the ONC of 2.06 pc, which partially incorporates OMC-2. Carpenter (2000) used the surface density of 2MASS sources on the sky, corrected for background contamination, to map the distribution of young stars in the Orion A cloud. Using a smoothed surface density plot, Carpenter (2000) identified clusters as contiguous areas of elevated surface density; this analysis led to the incorporation of the OMC-2/3 and NGC 1977 regions into a single cluster centered on the Orion Nebula, four parsecs in radius, with over 1700 stars. More recently, Megeath et al. (2008a, in prep; see also Allen et al. (2007)) used the path linkage criterion of Battinelli (1991) with a critical length of 0.33 pc to map the extent of the Orion Nebula cluster; they also include OMC-2/3 and NGC 1977 in the ONC.

In summary, the OMC-2/3 and NGC 1977 regions appear to be part of a complex of young stars and gas extending three parsecs from the Orion Nebula. These regions can be thought of as composing a continuous cluster of young stars. Observationally, these three regions are best differentiated by the morphologies of their 8  $\mu\text{m}$  nebulosity. The Orion Nebula is characterized by bright emission due to OB stars heating the surface of the Orion A cloud; in this region, the molecular cloud appears to be behind the bright nebulosity. In contrast, the OMC-2/3 region shows the molecular gas in absorption against extended diffuse emission. Finally, the NGC 1977 region is surrounded by a loop of emission; presumably the walls of a cavity cleared in the molecular gas by the young B stars. The distinctive morphologies reflect the different environmental conditions in these three regions: the ONC region containing young stars and molecular gas irradiated by intense extreme UV radiation, the OMC-2/3 region containing protostars embedded in molecular filaments, and the NGC 1977 region being largely cleared of molecular gas and containing young stars irradiated by far-UV radiation from three

B stars. These different environmental conditions are perhaps the best motivation for dividing the northern end of the Orion A cloud into three distinct regions.

### 3. The Orion Molecular Cloud 2/3 Region

The OMC-2/3 region (see Figures 3 and 4) encompasses a section of the Orion A molecular cloud undergoing vigorous star forming activity, and at a distance of 450 pc (Genzel & Stutzki 1989), it contains one of the richest assemblages of protostars in the extended solar neighborhood. It is important to note that four recent and independent estimates of the distance to the ONC place it closer, consistent with a value of 420 pc (Hirota et al. 2007; Jeffries 2007; Menten et al. 2007; Sandstrom et al. 2007); however, throughout this discussion we use 450 pc.

OMC-2/3 is located in a molecular filament extending northward from the Orion Nebula (NGC 1976) to NGC 1977. Interest in OMC-2/3 was elevated by the detection of a chain of 21 submillimeter condensations by Chini et al. (1997) and the detection of numerous knots of H<sub>2</sub> emission from multiple outflows (Yu, Bally, & Devine 1997). These observations revealed for the first time the full extent of the star formation activity in OMC-2/3.

The OMC-2 region was first defined by Gatley et al. (1974) in their discovery of a group of near-infrared sources embedded in a molecular core, centered at a position of  $\alpha = 05^h 35^m 26.8^s$ ,  $\delta = -05^\circ 10' 17''$  (J2000). The far-infrared luminosity of OMC-2 is estimated to be  $2 \times 10^3 L_\odot$  (Thronson et al. 1978). OMC-2 is north of OMC-1, which is the molecular cloud associated with the Orion Nebula. Interestingly, the discovery of OMC-3 is not well documented in the literature. In Morris et al. (1974), reference is made to a secondary maximum 11' north of OMC-2 in a map of HCN  $J = 1 \rightarrow 0$  emission that was possibly an artifact due to the large, 2' beamwidth. Two years later, Kutner, Evans, & Tucker (1976) also appear to detect a maximum north of OMC-2 in 2 millimeter H<sub>2</sub>CO emission at the same beamwidth, but at a distance of 16'. The first actual reference to "OMC-3" occurs in Thronson et al. (1978) where far-infrared observations of OMC-3 were centered approximately on  $\alpha = 05^h 35^m 10.3^s$ ,  $\delta = -04^\circ 55' 01''$  (J2000), which is almost 16' north of OMC-2. Goudis (1982) also notes that OMC-3 is 16' north of OMC-2; a reference is not given but presumably it is based on this observation. Since that time, most of the references to OMC-3 have referred to the location of the secondary maximum in the HCN map from the initial Morris et al. (1974) paper of 11' north of OMC-2. In particular, Chini et al. (1997) define OMC-3 as the region between 3' and 11' north of the center of OMC-2.

In the remainder of this section, we will define the OMC-2/3 as the gas and associated stars within the  $20' \times 20'$  field outlined in Figure 2. This is the region mapped by Peterson et al. (2008) in their deep, near-infrared observation of OMC-2/3 (Figures 3 and 4), and encompasses the protostellar and prestellar sources detected in the submillimeter surveys.

#### 3.1. Molecular Gas

The Bally et al. (1987) Bell Labs survey of <sup>13</sup>CO  $1 \rightarrow 0$  emission extensively mapped the Orion A molecular cloud covering 8 deg<sup>2</sup>; the total mass was found to be  $5 \times 10^4 M_\odot$ . The map shows an integral shaped filament in the northern part of the Orion A cloud from NGC 1977 in the north through the Orion Nebula in the middle down to about 20' north of NGC 1999 in the south. This filament, which includes OMC-2/3, is about

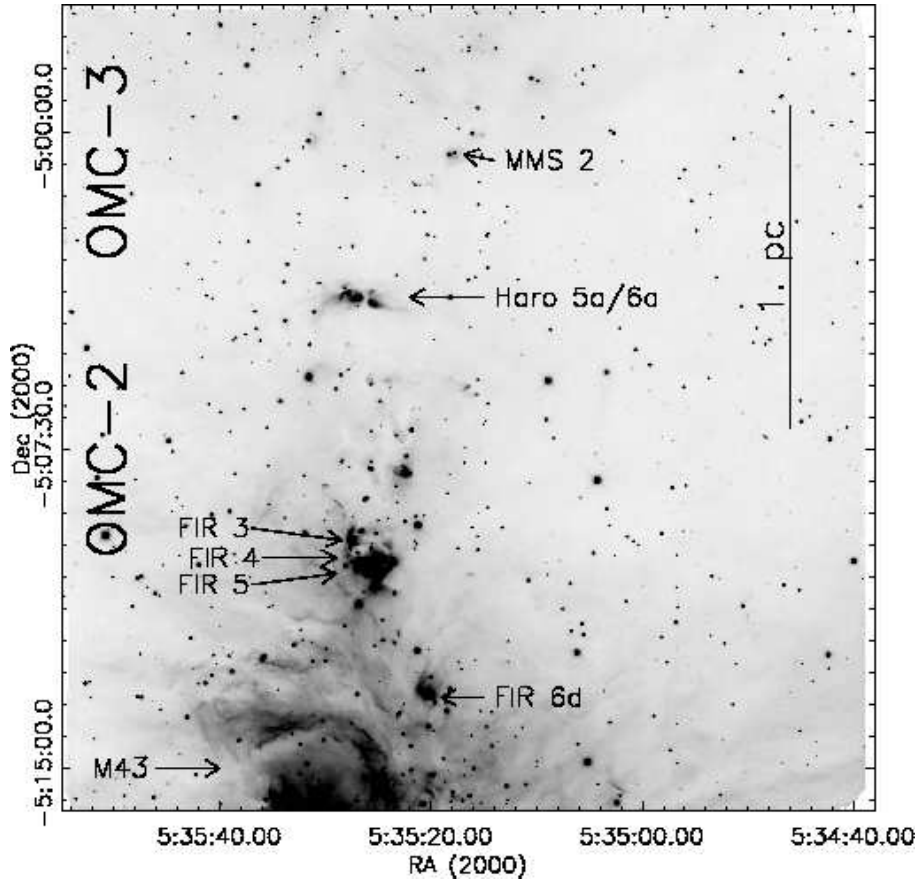


Figure 3. OMC-2/3. The  $20' \times 20'$   $K$ -band field mapped by Peterson et al. (2008) in their near-infrared study of OMC-2/3. Sources discussed in the text which are prominent in this image are labeled.

$0.5 \times 13$  pc long and has a total mass of  $5 \times 10^3 M_{\odot}$ , or about 25% of the total mass of their map of the Orion A cloud. Bally et al. (1987) suggest that the filament results from the interstellar medium being compressed by a superbubble driven by the Orion OB association.

Dutrey et al. (1993) obtained  $J = 2 \rightarrow 1$   $C^{18}O$  maps of the Orion A cloud and found that the filament seen in the Bally et al. (1987) map breaks up into several discrete fragments. From these observations, the molecular gas masses of OMC-2 and OMC-3 are found to be  $113 M_{\odot}$  and  $140 M_{\odot}$ , respectively. However, a higher resolution study by Castets & Langer (1995) in several transitions of  $^{13}CO$ ,  $C^{18}O$ ,  $C^{32}S$  and  $C^{34}S$  shows both these regions to be much more complex. Castets & Langer (1995) shows a single dense core in OMC-2 with a mass of  $22 M_{\odot}$  and a radius of 0.11 pc. In contrast, they find the gas traced by  $C^{18}O$  and CS in OMC-3 is highly elongated with a total mass of  $55 M_{\odot}$ . The CS observations show three dense cores in OMC-3 with masses of 12, 10 and  $13 M_{\odot}$ ; since CS traces only the dense gas, it is inferred that the  $C^{18}O$  maps are detecting a massive envelope surrounding the dense cores.

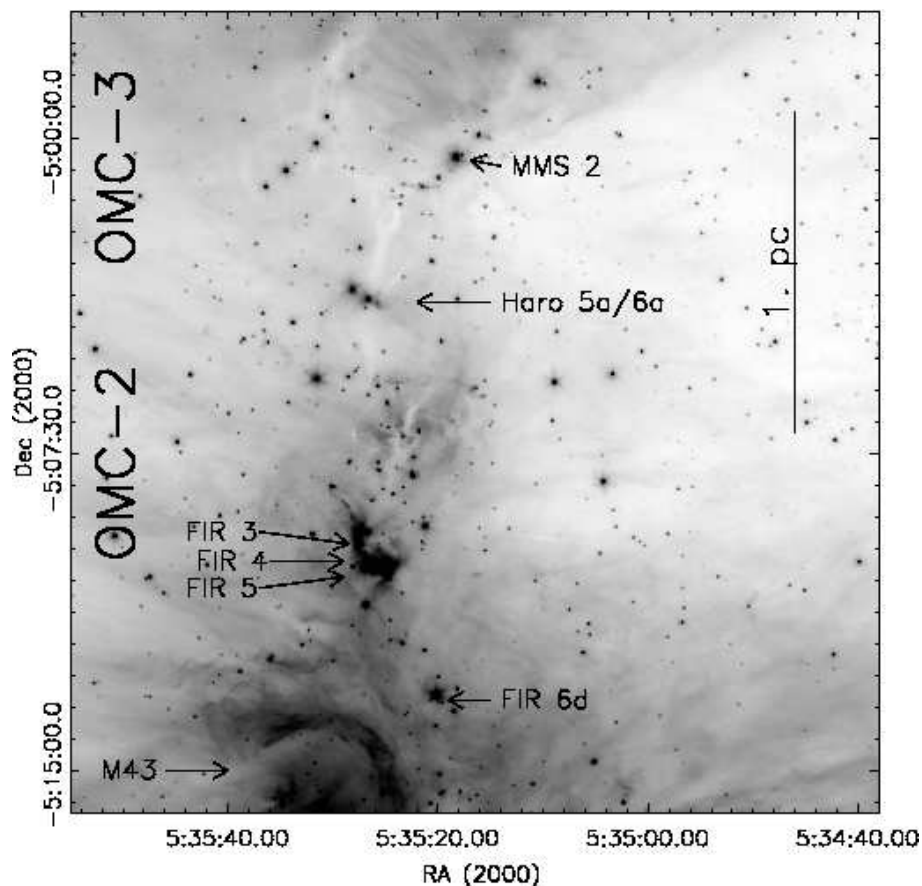


Figure 4. OMC-2/3. A  $20' \times 20'$  image showing  $4.5 \mu\text{m}$  band emission observed with the IRAC camera on board the *Spitzer* Space Telescope. This is the same region shown in Figure 3, and the annotations from Figure 3 are displayed.

### 3.2. Submillimeter Sources

Submillimeter observations of OMC-2/3 have been conducted at  $1300 \mu\text{m}$  (Mezger, Wink, & Zylka 1990; Chini et al. 1997; Nielbock, Chini, & Müller 2003),  $850 \mu\text{m}$ ,  $450 \mu\text{m}$  (Johnstone & Bally 1999), and  $350 \mu\text{m}$  (Lis et al. 1998), resulting in the discovery of a wealth of pre-stellar, Class 0 and Class I objects. Twenty-one compact sources were detected in OMC-2/3 by Chini et al. (1997) in their  $1300 \mu\text{m}$  dust imaging of the region. Previous to Chini et al. (1997), the OMC-2 core was observed at  $1300 \mu\text{m}$  by Mezger, Wink, & Zylka (1990) and their original six sources, listed as FIR 1a, 2–5 and 6a in Table 1, were also detected by Chini et al. (1997). In OMC-2, Chini et al. (1997) detected two additional sources north of FIR 1a (FIR 1b and 1c) as well as a cluster of compact sources near FIR 6a: FIR 6b–6e. Finally, Chini et al. (1997) found four more sources in OMC-2 (MMS 7-10) and six sources in OMC-3 (MMS 1-6). Based on  $L_{\text{bol}}/L_{\text{submm}}$  ratios  $< 200$ , all six condensations in OMC-3 fit the definition of Class 0 objects, and are thus in the earliest stages of protostellar evolution (Chini et al. 1997).

All 21 sources of Chini et al. (1997) were detected at  $350 \mu\text{m}$  by Lis et al. (1998) except for one (MMS 10), and an additional 13 sources were discovered (CSO 1–33

Table 1. Submillimeter Sources in OMC-2/3

Source Name <sup>b</sup>	R.A. <sup>a</sup> (J2000)	Dec. <sup>a</sup> (J2000)	S (350 $\mu$ m) (Jy)	S (1300 $\mu$ m) (mJy)	S (3.6 cm) (mJy)	Other Designations <sup>b</sup>
MIR 1/2	05 35 28.3	-04 58 38		290		
CSO 1	05 35 29.8	-04 58 47	15			
CSO 2	05 35 13.9	-04 59 25	15			
MIR 3	05 35 15.8	-04 59 59	17	179		CSO 3
CSO 4	05 35 17.1	-05 00 03	19			
MMS 1	05 35 18.1	-05 00 20	26	347		CSO 5
MMS 2	05 35 18.5	-05 00 30	25	249	0.25	CSO 6; VLA 1; MIR 5/6
MMS 3 <sup>c</sup>	05 35 19.2	-05 00 51	26	152		CSO 7
MMS 4	05 35 20.5	-05 00 50.0	27	354		CSO 8; MIR 7
MMS 5	05 35 22.5	-05 01 15	24	400		CSO 9
MMS 6	05 35 23.5	-05 01 31	45	2000	0.15	CSO 10; VLA 3
CSO 11	05 35 27.1	-05 03 39	15	164		MIR 9
MMS 7	05 35 26.5	-05 03 57	19	360	0.59	CSO 12; VLA 4; MIR 10; IRAS 05329-0505
MMS 8	05 35 26.7	-05 05 19	17	268		CSO 13
MMS 10	05 35 32.3	-05 05 42		166		
MMS 9	05 35 26.2	-05 05 44	21	412	0.79	CSO 14, VLA 5
MIR 11	05 35 31.5	-05 05 47		228		
MIR 12	05 35 25.8	-05 05 58		146		
CSO 15	05 35 22.9	-05 06 41	14			
FIR 1c	05 35 23.8	-05 07 09	18	180		CSO 16; MIR 14; IRAS 05329-0508
FIR 1b	05 35 23.7	-05 07 35	18	195		CSO 17
FIR 1a	05 35 24.4	-05 07 53	18	393	0.31	CSO 18; VLA 8 <sup>d</sup>
CSO 19	05 35 25.0	-05 08 19	15			
CSO 21	05 35 26.4	-05 08 26	14			
FIR 2	05 35 24.4	-05 08 34	17	340		CSO 20; MIR 19
MIR 20	05 35 26.9	-05 09 24		351		
FIR 3	05 35 27.5	-05 09 38	36	676	2.48	CSO 22; VLA 11; MIR 21/22
FIR 4	05 35 26.8	-05 10 03	67	1252	0.64	CSO 23; VLA 12; MIR 24?; IRAS 05329-0512
MIR 25	05 35 27.6	-05 10 09		216		
MIR 26	05 35 28.2	-05 10 14		423		
FIR 5	05 35 26.4	-05 10 24	34	452		CSO 24; MIR 27?
MIR 28	05 35 24.8	-05 10 30		186	1.04	VLA 13
FIR 6b	05 35 23.3	-05 12 09	15	300		CSO 25; MIR 29
CSO 26	05 35 26.3	-05 12 23	14			
CSO 27	05 35 24.7	-05 12 33	19			
FIR 6a	05 35 23.4	-05 12 42	21	361		CSO 28
MIR 30	05 35 18.2	-05 13 07		186		
FIR 6c	05 35 21.6	-05 13 14	18	450		CSO 29
FIR 6d	05 35 19.8	-05 13 19	12	314		CSO 30; MIR 31/32
MIR 36	05 35 22.6	-05 14 11		184		
CSO 31	05 35 21.5	-05 14 30	15	189		MIR 37
CSO 32	05 35 21.3	-05 14 54	15	161		MIR 38
MIR 39/40	05 35 19.9	-05 15 09		140		
MIR 41	05 35 23.5	-05 15 23		42		
CSO 33	05 35 19.5	-05 15 35	20	288		MIR 42
MIR 43/44	05 35 25.3	-05 15 36		48		

<sup>a</sup> Positions from Lis et al. (1998) except for source 15 which has Chini et al. (1997) coordinates. For non-CSO or MMS sources, MIR coordinates are used (Nielbock, Chini, & Müller 2003).

<sup>b</sup> CSO names and corresponding fluxes from Lis et al. (1998), MMS and FIR from Chini et al. (1997), VLA from Reipurth, Rodríguez, & Chini (1999) and MIR from Nielbock, Chini, & Müller (2003). IRAS sources from the Point Source Catalog. The 350  $\mu$ m and 1300  $\mu$ m positions agree to within  $\lesssim 6''$  (Lis et al. 1998).

<sup>c</sup> There is a positional difference between CSO 7 and MMS 3 of  $\sim 19''$ ; consequently, the association of these sources is uncertain. Coordinates are from Lis et al. (1998).

<sup>d</sup> There is a positional difference between FIR 1a and VLA 8 of  $\sim 8''$ ; however, FIR 1a has a broad peak and VLA 8 is located within the boundary so the association is likely (Reipurth, Rodríguez, & Chini 1999).

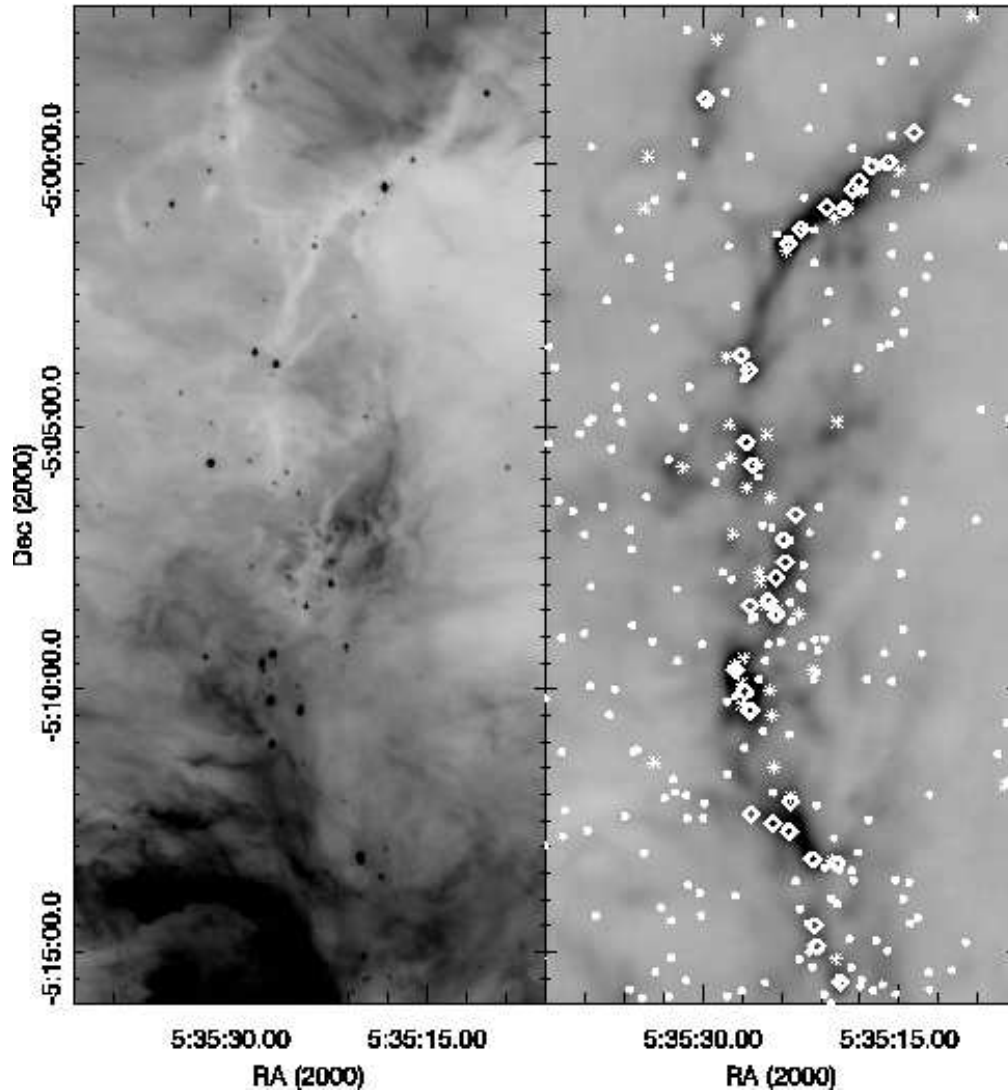


Figure 5. The central part of the OMC-2/3 region shown in Figure 3. The left panel shows the *Spitzer* 8  $\mu\text{m}$  map. The right panel shows the 850  $\mu\text{m}$  map of Johnstone & Bally (1999) in inverse greyscale. Overlaid on this map are the following: 1.) positions of the 34 submillimeter sources given in Table 1 (diamonds), 2.) positions of *Spitzer* identified protostellar candidates (asterisks) and 3.) positions of pre-main sequence stars (circles; see Section 3.4.). Note that many of the filaments seen in emission in the 850  $\mu\text{m}$  map are seen in absorption against the diffuse background in the 8  $\mu\text{m}$  map.

in Table 1). In Figure 5, these 34 submillimeter sources are shown with the 8  $\mu\text{m}$  IRAC map as well as the 850  $\mu\text{m}$  map from Johnstone & Bally (1999). Overall, the submillimeter sources follow the filamentary structure of the 850  $\mu\text{m}$  emission.

Nielbock, Chini, & Müller (2003) also obtained 1300  $\mu\text{m}$  maps of OMC-2/3 and identified 12 new 1300  $\mu\text{m}$  peaks in addition to the ones already identified; all are

listed in Table 1 (MIR sources). They complemented the submillimeter data with mid-infrared imaging and detected at least 13 (and as many as 15) of the submillimeter peaks at  $11.9 \mu\text{m}$  ( $N$ -band) and  $17.8 \mu\text{m}$  ( $Q$ -band). In the mid-infrared, 6 of the submillimeter peaks are resolved into double sources, e.g. MMS 2 from Chini et al. (1997) is resolved into MIR 5 and 6 (Nielbock, Chini, & Müller 2003). The projected spatial separation of these two particular sources is  $1.3''$ , or 570 AU at 450 pc, with a position angle of  $45^\circ$ .

Two of the submillimeter sources of Chini et al. (1997) coincide with Infrared Astronomical Satellite (IRAS) sources: IRAS 05329–0505 (MMS 7) and IRAS 05329–0512 (FIR 4). There are also two submillimeter sources detected in X-rays: MMS 2 and 3 (Tsuboi et al. 2001).

Seven of the Chini et al. (1997) sources were also detected at 3.6 cm (Reipurth, Rodríguez, & Chini 1999). They present radio continuum maps and detect a total of 14 sources at 3.6 cm, where 3 are likely background sources. The remaining 11 are likely either young stars or protostars. Of those 11 sources, 7 are also detected at  $1300 \mu\text{m}$  and are listed in Table 1 (VLA 1, 3, 4, 5, 8, 11, 12). These centimeter sources are thought to result from ionized gas in outflows, and they are clear evidence that many of the submillimeter sources are indeed protostars containing hydrostatic cores (Reipurth, Rodríguez, & Chini 1999).

Submillimeter wavelength polarimetry of OMC-3 has shown that the magnetic field is perpendicular to the filament along most of the length of the region encompassed by the MMS 1-9 cores (Matthews & Wilson 2000). They also find that the outflows in this region are not consistently aligned with the ambient field or the filament.

### 3.3. Outflows

Infrared, optical and millimeter measurements have shown that OMC-2/3 is rich with outflows driven by the young stars in this region. Yu, Bally, & Devine (1997, hereafter, YBD97) discovered 80 knots from  $2.12 \mu\text{m}$  imaging of the  $v = 1 - 0$  S(1) line of shock excited  $\text{H}_2$  with nearly a dozen of those being collimated outflows from young stellar objects (YSOs) in OMC-2/3. Observations in  $^{12}\text{CO } J = 2 \rightarrow 1$  by Yu et al. (2000) suggest that these  $\text{H}_2$  knots are driving molecular outflows. OMC-2/3 was also observed at  $2.12 \mu\text{m}$  by Stanke, McCaughrean, & Zinnecker (2002, hereafter SMZ02) and they identified 24 flows labeled SMZ 2–25. Tables 2 and 3 in SMZ02 enumerate the flows (Table 3) and each of the  $\text{H}_2$  knots associated with those flows (Table 2); Table 2 also includes a comprehensive correlation of the HH objects and YBD97  $\text{H}_2$  knots with the SMZ02  $\text{H}_2$  features. Using these positions, Williams, Plambeck, & Heyer (2003) identified nine outflows in CO emission from high resolution Berkeley-Illinois-Maryland Array (BIMA) imaging. Figure 7, from Williams, Plambeck, & Heyer (2003), shows the location of those nine outflows, each of which appears to originate from a Chini et al. (1997) submillimeter source. The nine outflows line up with approximately 50 of the 60 YBD97  $\text{H}_2$  knots that are coincident with the BIMA map; those that do not are likely to be outflows in the plane of the sky (Williams, Plambeck, & Heyer 2003). Aso et al. (2000) identified 4 additional molecular outflows from CO ( $1 - 0$ ) and  $\text{HCO}^+$  ( $1 - 0$ ) observations with the Nobeyama 45-m telescope, and all are associated with the known far-infrared or millimeter sources (Chini et al. 1997; Lis et al. 1998).

The most prominent Herbig Haro objects in OMC-2/3 are associated with the bipolar reflection nebula known as Haro 5a/6a, first noted by Haro (1953). Haro 5a/6a appears almost edge-on (see Figures 3, 4, & 6), exhibiting a dark lane between the two lobes of the nebula at optical and near-infrared wavelengths (YBD97; SMZ02). A

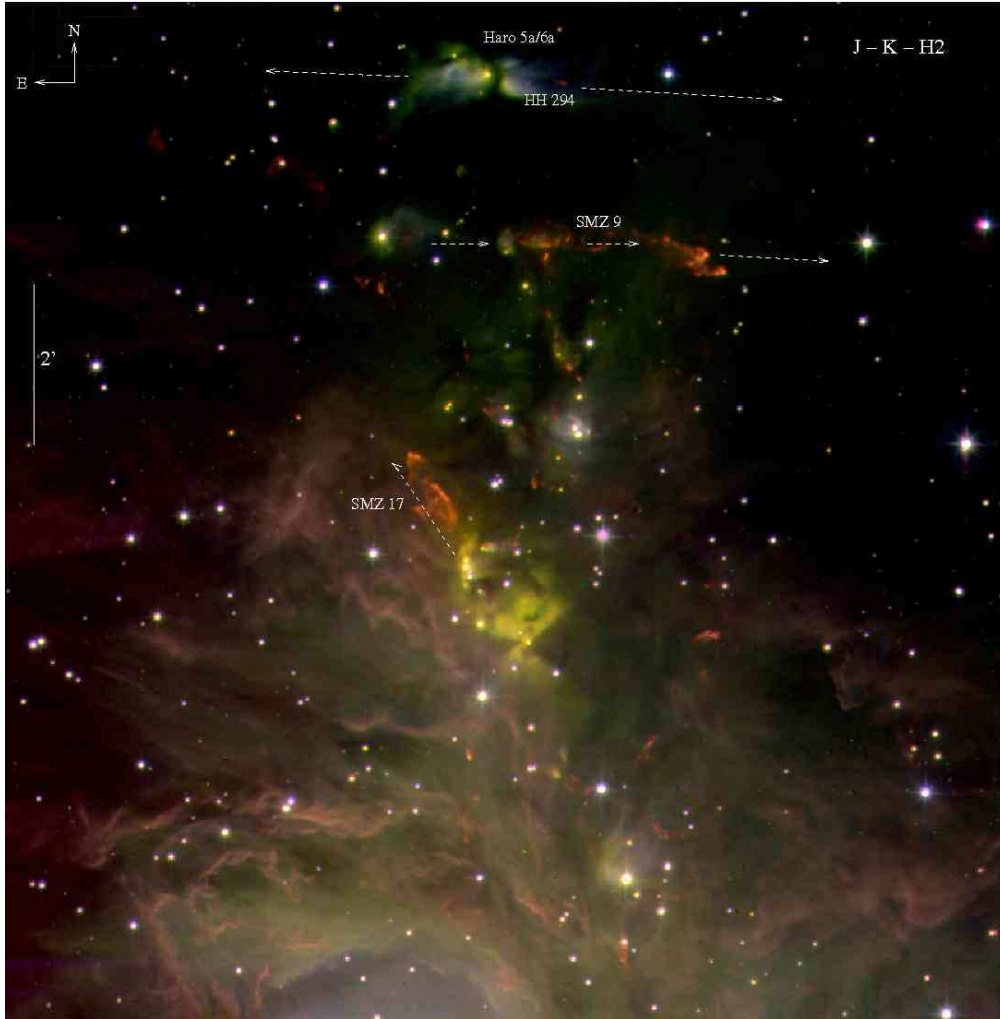


Figure 6. Near-infrared J-K-H<sub>2</sub> color-composite image of the OMC-2/3 region. Jets and outflows appear in red. The flow associated with Haro 5a/6a is SMZ 6. Data obtained with the wide-field imager, WFCAM, on UKIRT. Figure courtesy of Chris Davis (private communication).

slightly tilted obscuring torus is inferred from imaging polarimetry data (Wolstencroft et al. 1986), while near-infrared spectroscopy suggests that the source hidden by the torus may be an FU Orionis type variable (Reipurth & Aspin 1997; Greene et al. 2008).

Haro 5a/6a is centered on IRAS source 05329-0505, which is one of the 1300  $\mu\text{m}$  sources (MMS 7) detected by Chini et al. (1997). It is also associated with a radio jet (Reipurth et al. 2004) and a large-scale bipolar outflow (Yu, Bally, & Devine 1997; Williams, Plambeck, & Heyer 2003). The western lobe of the nebula (Haro 5a) includes a knot of H<sub>2</sub> emission coinciding with HH 294 (see our Table 2 for a list of the prominent outflows in OMC-2/3), a well collimated optical jet 100'' in length which flows from the IRAS source (Reipurth, Bally, & Devine 1997). The flow axis intercepts more distant HH knots 42, 128, and 295 (Ogura & Walsh 1991; Reipurth, Bally, & Devine

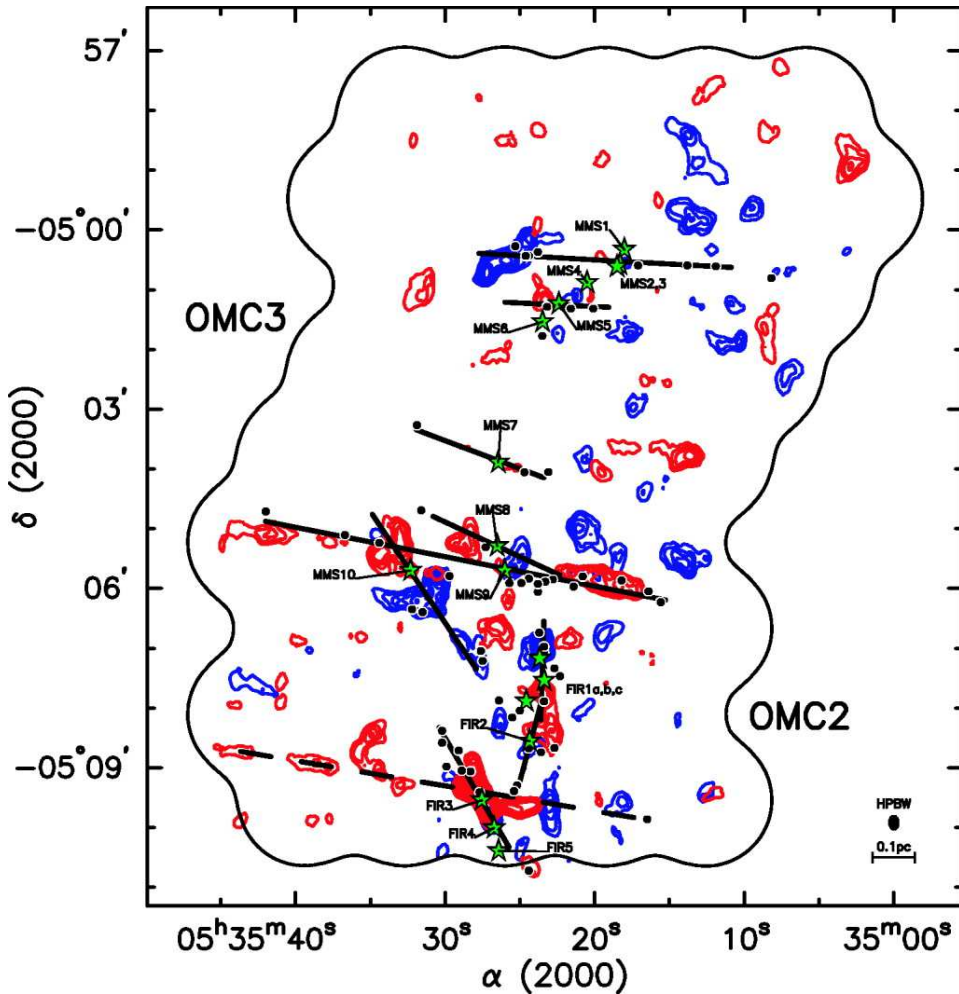


Figure 7. This figure from Williams, Plambeck, & Heyer (2003) shows line-wing emission from their BIMA mosaic (interferometer data only). The blue and red contours show emission integrated from  $v = 5.5$  to  $9.0 \text{ km s}^{-1}$  and  $12.5$  to  $16.0 \text{ km s}^{-1}$ , respectively. The contour starting levels and increments are the same ( $8, 4 \text{ K km s}^{-1}$ ) for both velocity ranges. The star symbols represent the positions of the Chini et al. (1997) submillimeter sources and dots represent the  $\text{H}_2$  knots from Yu, Bally, & Devine (1997). The solid contour around the map is the 30% sensitivity level and the  $8.8'' \times 13.4''$  beam is shown in the lower right-hand corner.

1997), although the complex web of flows in this region makes concrete associations difficult – particularly at infrared and millimeter wavelengths (Schwartz, Burton & Herrmann 1997; Yu, Bally, & Devine 1997; Yu et al. 2000; Stanke, McCaughrean, & Zinnecker 2002; Williams, Plambeck, & Heyer 2003; Davis et al. 2008, in prep; see also Figures 6 & 7). Large, though faint,  $\text{H}_2$  bow shocks are detected by SMZ02, which they associate with flow SMZ 6 originating from Haro 5a/6a (also called flow “F” in YBD97). This source has also been detected in  $3\text{--}24 \mu\text{m}$  *Spitzer* observations and is classified as a protostar on the basis of the *Spitzer* photometry (see Section 3.4.).

About  $3'$  north of Haro 5a/6a, a compact chain of optical/infrared knots trace HH 293 (flow SMZ 5 in SMZ02; flow “C” in YBD97). Bright  $H_2$  bows delineate a third flow  $\sim 2'$  to the south of Haro 5a/6a (flow SMZ 9 in SMZ02; flow “H” in YBD97; labeled in Figure 6). A fourth  $H_2$  flow (flow SMZ 3 in SMZ02; flow “B” in YBD97) is detected a further arcminute north-west of HH 293. Notably, all four flows are more-or-less parallel, and orthogonal to the chain of cores that runs roughly north-south through the center of the region. Further south toward FIR 4 and the region directly west of M 43, a complex of star forming cores produces at least another half-dozen  $H_2$  flows (Yu et al. 2000; Stanke, McCaughrean, & Zinnecker 2002; Davis et al. 2008), although these are more randomly oriented. Chini et al. (1997), Yu et al. (2000) and Williams, Plambeck, & Heyer (2003) present molecular line maps of the outflows in this region. The extremities of many of the flows in this region, where they break out of the north-south molecular filament that pervades OMC-2/3, are manifest as optically-visible HH objects (Ogura & Walsh 1991; Reipurth, Bally, & Devine 1997).

Table 2. Prominent Herbig-Haro and  $H_2$  outflows in OMC-2/3

HH or $H_2$ designation <sup>a</sup>	Driving source <sup>b</sup>	RA <sup>c</sup> (2000)	Dec <sup>c</sup> (2000)	Other flow designations	Length (pc) <sup>d</sup>	Refs <sup>e</sup>
HH 294	IRAS05329-0505; MMS 7	05 35 26.4	-05 03 54	Haro 5a/6a; SMZ 6; YBD “F”	1.43	1,2,3,4
HH 293	MMS 5	05 35 22.4	-05 01 16	SMZ 5; YBD “C”	0.05	1,3,4
SMZ 9	MMS 9	05 35 26.2	-05 05 46	YBD “H”	0.34	3,4
SMZ 3	IRS 1	05 35 18.2	-05 00 33	YBD “B”	0.70	3,4

<sup>a</sup> SMZ refers to the  $H_2$  flow nomenclature of Stanke, McCaughrean, & Zinnecker (2002).

<sup>b</sup> MMS designations from Chini et al. (1997).

<sup>c</sup> Positions for each flow from Table 3 in Stanke, McCaughrean, & Zinnecker (2002).

<sup>d</sup> Jet length from Stanke, McCaughrean, & Zinnecker (2002) assuming a distance to Orion A of 450 pc.

<sup>e</sup> References: (1) Reipurth, Bally, & Devine (1997), (2) Davis et al. (2008), (3) Stanke, McCaughrean, & Zinnecker (2002), (4) Yu, Bally, & Devine (1997).

### 3.4. Pre-main Sequence Stars and Infrared Selected Protostars

In the discovery paper of OMC-2, Gatley et al. (1974) presented a  $2.2 \mu\text{m}$  map of OMC-2 showing five bright sources surrounded by nebulosity, four without optical counterparts. Observations from 1.6 to  $20 \mu\text{m}$  showed that these sources had rising spectral energy distributions. Rayner et al. (1989) published the first infrared array observations of OMC-2 at  $1-3 \mu\text{m}$ , including polarimetry which showed that the four infrared sources were the source of the reflection nebulosity associated with the sources. Infrared photometry by Johnson et al. (1990) found luminosities of 20 to  $1000 L_{\odot}$  for these sources.

The first wide-field infrared map of OMC-2/3 was a  $15' \times 5'$   $JHK$  mosaic by Jones et al. (1994) which showed OMC-2 as a small group of red sources surrounded by an extended and relatively uniform distribution of stars. They argued that the majority of the 219 sources were associated with the Orion cloud, and were not background stars; this is the first evidence of a large population of stars associated with OMC-2.

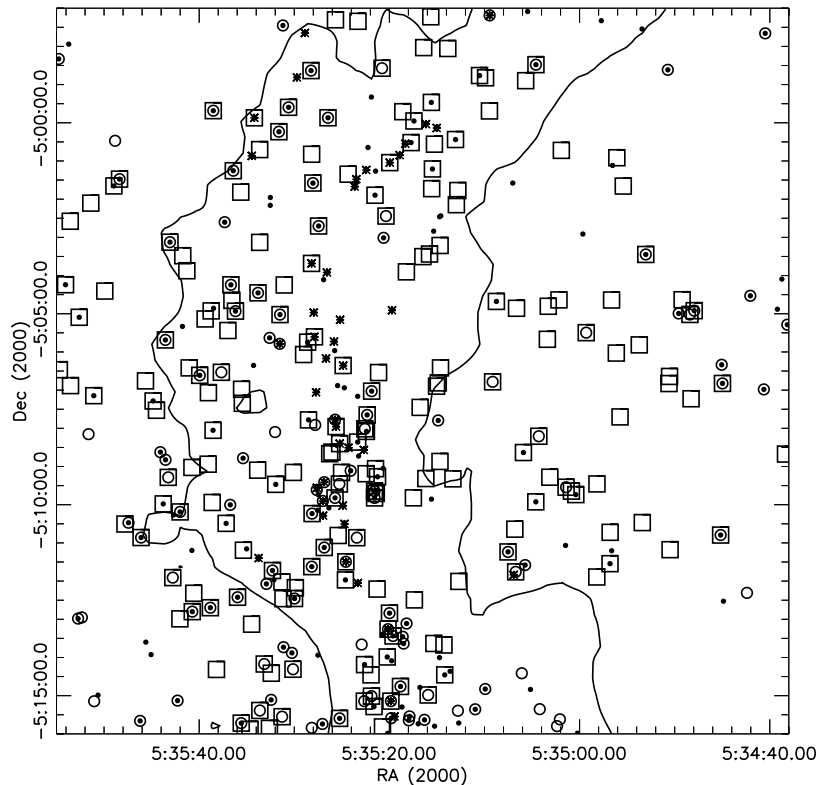


Figure 8. The pre-main sequence star population in OMC-2/3 overlaid on the CS  $2 \rightarrow 1$  emission (N. Ridge, priv. comm.). The sources represented by dots are those with infrared excess, asterisks are the infrared-selected protostars, open circles are the Carpenter, Hillenbrand, & Skrutskie (2001) variables, and squares are infrared sources with X-ray emission detected by Chandra (Tsujiimoto et al. 2002).

Ali & DePoy (1995) mapped OMC-2 as part of a  $2.2 \mu\text{m}$  survey of the Orion A molecular cloud. Their surface density maps showed OMC-2 as a distinct density peak about  $15'$  north of the center of the ONC; within this density peak they found  $\sim 30$  sources. They also noted the presence of a large distributed population surrounding the ONC and OMC-2 regions containing around  $\sim 1500$  members. Nielbock, Chini, & Müller (2003) combined mid-infrared imaging with the 2MASS point source catalog and found 57 sources with infrared excess in the OMC-2 and OMC-3 regions. Using the 2MASS point source catalog, they identified 260 possible young stars in the OMC-2 and OMC-3 regions, and found that the absolute  $J$ -band magnitude distribution of sources in OMC-2 peaked at a higher luminosity than that for OMC-3. It is not clear if this difference is due to a different distribution of stellar masses or different age distributions; hopefully, future spectroscopic observations can be used to search for variations in the mass spectrum.

Recent infrared and X-ray observations of the OMC-2/3 region motivate a re-examination of its population of pre-main sequence stars and protostars. These include the 2MASS survey of Orion, multi-epoch near-infrared imaging by Carpenter, Hillenbrand, & Skrutskie (2001), a 100 kilosecond Chandra integration by Tsujimoto et al. (2002), and finally, a wide field *Spitzer* survey of the Orion molecular clouds (Megeath et al. 2008a, in

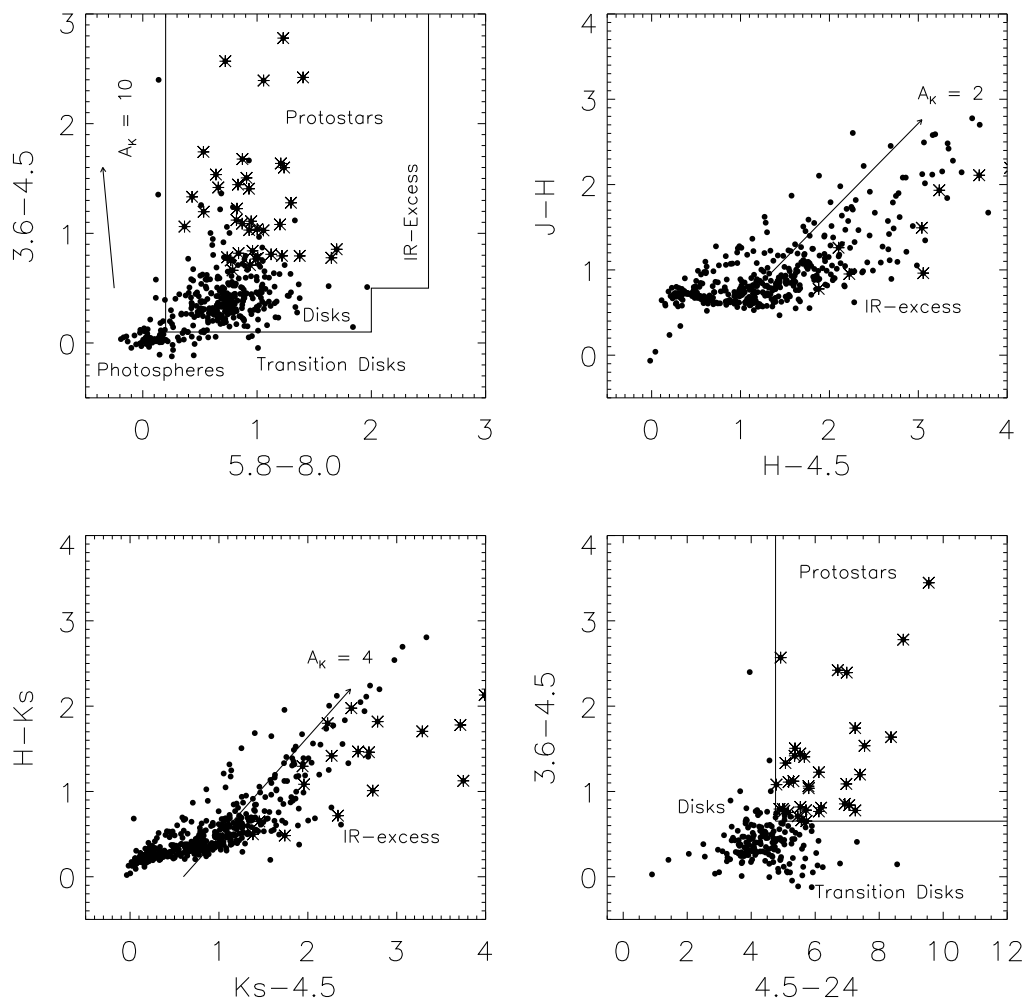


Figure 9. Color-color diagrams of YSOs in OMC-2/3 and NGC 1977 drawn from 2MASS and *Spitzer* photometry (Megeath et al. 2008a, in prep). The YSOs are identified either by infrared excesses, variability, or, in the case of OMC-2/3, X-ray emission. In the upper left diagram, we show the region of the 3.6–4.5 versus 5.8–8.0 color-color diagram populated by young stars with disks and protostars (Allen et al. 2004; Megeath et al. 2004; Winston et al. 2007). For sources not detected at 5.8 and 8.0  $\mu\text{m}$ , sources with infrared excesses due to disks and/or envelopes were identified by combining 4.5  $\mu\text{m}$  photometry with near-infrared 2MASS  $J$ ,  $H$ ,  $K_S$  photometry (Gutermuth et al. 2004; Winston et al. 2007). As shown in the upper right and bottom left diagrams, the infrared excess sources can be separated from reddened photospheres using the reddening vector from Flaherty et al. (2007). Additional transitional disk sources were identified using the 8.0–24 color (Muzerolle et al. 2004; Winston et al. 2007; Megeath et al. 2008a, in prep, with modified criteria); these are grouped with the stars with disks in our classification scheme. The bottom right shows the 3.6–4.5 versus 4.5–24 color-color diagram used to find likely protostars by identifying sources with mid-infrared colors consistent with a flat or rising spectral energy distribution (Megeath et al. 2008b, in prep).

prep). Using catalogs derived from these observations, we select young stellar objects as sources satisfying one of the following criteria: 1) presence of a mid-infrared excess from a dusty disk or envelope (Allen et al. 2004; Megeath et al. 2004; Gutermuth et al. 2004; Winston et al. 2007; Whitney et al. 2004; Megeath et al. 2008a,b, in prep; Figure 9), 2) variability in the near-infrared (Carpenter, Hillenbrand, & Skrutskie 2001), or 3) X-ray emission from an infrared source detected by *Spitzer* and/or 2MASS. We note that deep near-infrared imaging by Tsujimoto et al. (2003) detected 74 X-ray sources which were not detected by 2MASS; we have not merged our data with their source list.

Using these criteria, we have identified 347 candidate member pre-main sequence stars and protostars. Table 3 shows photometry for the young stellar object candidates that are detected at  $24\ \mu\text{m}$ . The X-ray sources are taken from a reprocessing of the Chandra data of Tsujimoto et al. (2002) for the ANCHORS database (An Archive of Chandra Observations of Regions of Star Formation, S. Wolk P. I.). In Figure 8, we show the distribution of these sources over the  $20' \times 20'$  field. These sources were also shown in Figure 5. In Figure 9, we show color-color diagrams of the sources. Out of 347 sources total, we identify 208 infrared excess sources. Of these, 43 sources with  $24\ \mu\text{m}$  detections are classified as protostars (Class 0/I). The remaining 165 are predominantly stars with disks (Class II), although there may also be some protostars without  $24\ \mu\text{m}$  detections among these stars. In addition, 123 sources exhibit variability in the near-infrared, and 197 have X-ray detections. A total of 139 sources exhibiting variability or X-ray emission do not have infrared excesses and thus appear to be pure photospheres in the infrared (Class III). These observations demonstrate the presence of a large number of pre-main sequence stars in the OMC-2/3 region. Future spectroscopic observations are needed to determine the ages and masses of these stars and determine the star forming history and initial mass function of the OMC-2/3 region.

### 3.5. Young Brown Dwarfs in OMC-2/3

In addition to a large population of pre-main sequence stars and protostars, a number of young brown dwarfs have been discovered in OMC-2/3. Table 4 lists the 19 spectroscopically confirmed young brown dwarfs from Peterson et al. (2008) along with their  $I$ - and  $z'$ -band magnitudes, deep near-infrared  $JHK$ -band magnitudes, and spectral types. The spectral types of these young brown dwarfs range from M6.5 to M9, which corresponds to approximate masses of  $0.075$ – $0.015\ M_{\odot}$  using the evolutionary models of Baraffe et al. (1998). At least one of these young brown dwarfs (source 21 in Table 4) has strong  $H\alpha$  emission, indicating that it is actively accreting.

Young brown dwarfs, with ages much less than 10 Myr, are much more luminous and thus easier to detect than field brown dwarfs (typically older than 1 Gyr). However, the near-infrared colors of young brown dwarfs are similar to those of very low mass stars, making it very difficult to identify brown dwarfs from near-infrared photometry alone. Therefore, techniques for identifying brown dwarfs in star forming regions (Luhman 1999; Muench et al. 2001) were applied by Peterson et al. (2008) to select brown dwarf candidates in OMC-2/3 from near-infrared and visible wavelength photometry. Once candidate brown dwarfs were selected, far-red ( $0.6$ – $1.0\ \mu\text{m}$ ) and near-infrared ( $0.8$ – $2.5\ \mu\text{m}$ ) spectroscopy was obtained and used to confirm the candidates as *bona fide* brown dwarfs.

Figure 10 is a  $K$  versus  $H-K$  color-magnitude diagram of all sources in OMC-2/3 from Peterson et al. (2008). Assuming an age of 1 Myr, Baraffe et al. (1998) isochrones

were used to select sources below the hydrogen burning limit as candidate brown dwarfs. For sources that were not as deeply embedded and detected in the  $I$ - and  $z'$ -bands, near-infrared plus visible wavelength photometry was used for selection. The sources confirmed by spectroscopy as brown dwarfs or low-mass stellar members are shown in Figure 10. Note that we have observed all brown dwarf candidates that fall below  $0.080 M_{\odot}$  and above  $0.050 M_{\odot}$  (for 1 Myr objects) with an extinction limit of  $4.5 < A_V < 14$ , making a complete sample within this regime. Figure 10 illustrates how spectroscopy is needed to confirm the mass of the object, with both young ( $< 1$  Myr) brown dwarfs found above the reddening vector for 1 Myr old  $0.08 M_{\odot}$  and older low-mass stellar members found below the vector. Interpretations for this apparent dispersion in near-infrared luminosities are discussed in Peterson et al. (2008).

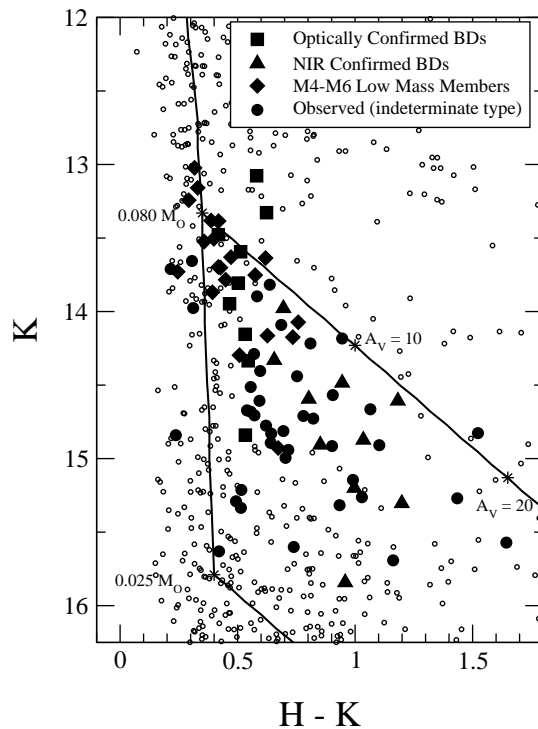


Figure 10.  $K$  vs.  $H - K$  color-magnitude diagram of all the stars detected at  $H$  and  $K$  in OMC-2/3 (small open circles) from Peterson et al. (2008). Over-plotted is the Baraffe et al. (1998) evolutionary isochrone for a 1 Myr-old pre-main sequence star, assuming a distance to OMC-2/3 of 450 pc. Reddening vectors are plotted for: 1) a  $0.08 M_{\odot}$  star (upper diagonal line) and 2) a  $25 M_J$  brown dwarf with an age of 1 Myr (lower diagonal line). The sources confirmed as brown dwarfs (spectral types of M6.5–M9) from far-red spectroscopy are represented by squares; those confirmed as low mass members (spectral types of M4–M6) are represented by diamonds. The sources confirmed as brown dwarfs from near-infrared spectroscopy are represented by triangles. All sources whose spectral types could not be determined or sources which were determined to be foreground or background dwarfs are represented by filled circles. Tables of photometry for all the sources whose spectra were obtained can be found in Peterson et al. (2008).

Table 3.: Young Stellar Object Candidates in OMC-2/3 detected at 24  $\mu\text{m}$ 

RA J(2000)	Dec J(2000)	$K_S^a$ mag (unc)	3.6 $\mu\text{m}$ mag (unc)	4.5 $\mu\text{m}$ mag (unc)	5.8 $\mu\text{m}$ mag (unc)	8 $\mu\text{m}$ mag (unc)	24 $\mu\text{m}$ mag (unc)	Var.	X-ray	IR-ex <sup>b</sup>	Proto.
5 35 19.5	-5 15 32			9.55 (0.01)	8.12 (0.01)	7.16 (0.03)	1.64 (0.03)	0	0	0	1
5 35 11.0	-5 15 21	11.12 (0.02)	9.23 (0.01)	8.46 (0.01)	8.10 (0.01)	7.71 (0.03)	4.32 (0.07)	1	0	1	0
5 35 19.8	-5 15 08	10.21 (0.03)	8.56 (0.01)	7.52 (0.01)	6.67 (0.01)	5.67 (0.02)	1.72 (0.03)	1	1	0	1
5 35 05.2	-5 14 50	7.19 (0.02)	6.99 (0.01)	6.67 (0.01)	6.39 (0.01)	5.97 (0.01)	3.71 (0.02)	0	0	1	0
5 35 20.2	-5 13 59	9.80 (0.02)	8.97 (0.01)	8.53 (0.01)	8.01 (0.01)	7.28 (0.03)	3.24 (0.02)	0	1	1	0
5 35 18.5	-5 13 38	9.29 (0.02)	7.73 (0.01)	7.03 (0.01)	6.16 (0.01)	5.27 (0.01)	1.79 (0.01)	1	0	1	0
5 35 45.6	-5 13 35	11.67 (0.02)	10.67 (0.01)	10.30 (0.01)	9.97 (0.01)	9.54 (0.07)	4.66 (0.05)	0	0	1	0
5 35 20.1	-5 13 15	6.43 (0.03)	6.16 (0.01)	4.48 (0.01)	3.67 (0.01)	2.80 (0.01)	-0.38 (0.02)	1	1	0	1
5 35 18.2	-5 13 06	9.64 (0.02)	8.67 (0.01)	8.19 (0.01)	7.83 (0.01)	7.16 (0.02)	3.84 (0.07)	1	0	1	0
5 35 52.7	-5 12 58	10.32 (0.02)	9.63 (0.01)	9.31 (0.01)	9.03 (0.01)	8.25 (0.01)	4.76 (0.06)	1	0	1	0
5 35 38.8	-5 12 41	8.82 (0.02)	7.97 (0.01)	7.57 (0.01)	6.96 (0.01)	6.25 (0.02)	3.72 (0.05)	1	1	1	0
5 34 44.9	-5 12 31	13.82 (0.04)	13.09 (0.02)	12.74 (0.02)	12.35 (0.10)		8.28 (0.02)	0	0	1	0
5 35 36.0	-5 12 25	8.39 (0.02)	7.17 (0.01)	6.52 (0.01)	6.04 (0.01)	5.30 (0.02)	2.70 (0.01)	1	1	1	0
5 35 32.9	-5 12 04	10.29 (0.02)	9.12 (0.01)	8.66 (0.01)	8.32 (0.01)	7.84 (0.03)	4.75 (0.04)	1	0	1	0
5 35 23.3	-5 12 03		10.49 (0.01)	8.96 (0.01)	8.58 (0.04)	7.94 (0.08)	1.41 (0.02)	0	0	0	1
5 35 06.9	-5 11 50			13.70 (0.04)			5.31 (0.07)	0	0	0	1
5 35 28.2	-5 11 37	11.32 (0.02)	10.54 (0.01)	10.10 (0.01)	9.65 (0.03)		4.74 (0.11)	1	1	1	0
5 35 05.7	-5 11 34	10.76 (0.02)	10.17 (0.01)	9.64 (0.01)	9.32 (0.01)	8.57 (0.04)	5.22 (0.04)	1	0	1	0
5 34 56.8	-5 11 32	10.15 (0.02)	8.87 (0.01)	8.57 (0.01)	8.19 (0.01)	7.45 (0.01)	4.55 (0.02)	0	1	1	0
5 35 24.6	-5 11 29	10.39 (0.02)	9.64 (0.01)	8.93 (0.01)	8.51 (0.01)	7.57 (0.03)	3.47 (0.02)	1	1	1	0
5 35 33.8	-5 11 23			13.30 (0.07)			5.30 (0.05)	0	0	0	1
5 35 07.5	-5 11 14	10.83 (0.02)	10.29 (0.01)	10.09 (0.01)	9.89 (0.01)	9.17 (0.05)	5.18 (0.09)	1	1	1	0
5 34 56.6	-5 11 12	12.20 (0.02)	11.44 (0.01)	10.94 (0.01)	10.58 (0.03)	9.86 (0.06)	6.31 (0.05)	0	0	1	0
5 35 26.8	-5 11 07	7.02 (0.03)	5.80 (0.01)	5.21 (0.01)	4.78 (0.01)	4.12 (0.01)	1.82 (0.08)	1	1	1	0
5 35 01.5	-5 11 03	12.23 (0.03)	11.63 (0.01)	11.20 (0.01)	10.81 (0.04)	9.54 (0.07)	6.27 (0.01)	0	0	1	0
5 35 46.1	-5 10 51	10.43 (0.02)	9.86 (0.01)	9.46 (0.01)	9.43 (0.01)	8.75 (0.03)	5.18 (0.01)	1	1	1	0
5 34 45.2	-5 10 47	10.70 (0.02)	10.15 (0.01)	9.77 (0.01)	9.63 (0.01)	9.13 (0.02)	6.11 (0.06)	1	1	1	0
5 35 24.7	-5 10 30	9.59 (0.07)	7.32 (0.01)	5.73 (0.01)	4.80 (0.01)	3.56 (0.01)	-1.40 (0.03)	0	0	0	1
5 35 47.4	-5 10 28	9.77 (0.03)	8.49 (0.01)	8.02 (0.01)	7.64 (0.01)	6.93 (0.01)	4.25 (0.02)	1	0	1	0
5 35 27.0	-5 10 17	8.80 (0.03)	5.83 (0.01)	4.81 (0.01)	3.69 (0.01)	2.63 (0.01)	-0.70 (0.50)	0	0	1	0
5 35 42.0	-5 10 11	9.47 (0.02)	8.73 (0.01)	8.42 (0.01)	8.00 (0.01)	7.42 (0.01)	4.56 (0.11)	1	1	1	0
5 35 24.9	-5 10 01	11.77 (0.19)	10.13 (0.05)	8.71 (0.03)	7.90 (0.02)	7.24 (0.03)	3.36 (0.01)	0	0	0	1
5 35 36.7	-5 10 00	11.94 (0.02)	11.04 (0.01)	10.53 (0.01)	10.11 (0.03)	9.25 (0.06)	6.17 (0.03)	1	0	1	0
5 35 04.6	-5 09 55	10.39 (0.02)	10.21 (0.01)	10.12 (0.01)	10.06 (0.01)	10.09 (0.07)	5.28 (0.02)	0	1	1	0
5 35 27.0	-5 09 54	12.75 (0.02)	10.23 (0.02)	9.00 (0.04)	8.13 (0.03)	7.31 (0.02)	2.89 (0.03)	1	0	0	1

<sup>a</sup> Magnitudes from 2MASS photometry.<sup>b</sup> From Carpenter, Hillenbrand, & Skrutskie (2001); Those that are variable have Stetson indices greater than 0.55.

Table 3.: Young Stellar Object Candidates in OMC-2/3 detected at 24  $\mu\text{m}$  (continued)

RA J(2000)	Dec J(2000)	$K_S^a$ mag (unc)	3.6 $\mu\text{m}$ mag (unc)	4.5 $\mu\text{m}$ mag (unc)	5.8 $\mu\text{m}$ mag (unc)	8 $\mu\text{m}$ mag (unc)	24 $\mu\text{m}$ mag (unc)	Var.	X-ray	IR-ex <sup>b</sup>	Proto.
5 35 15.6	-5 09 51	11.54 (0.02)	10.55 (0.01)	10.04 (0.01)	9.57 (0.01)	8.92 (0.03)	5.57 (0.03)	0	0	1	0
5 35 25.7	-5 09 49	10.11 (0.02)	9.61 (0.01)	9.56 (0.03)	9.27 (0.05)	8.34 (0.06)	3.63 (0.01)	1	1	1	0
5 35 21.6	-5 09 49	11.67 (0.02)	10.80 (0.01)	10.40 (0.01)	10.06 (0.02)	9.18 (0.04)	5.73 (0.06)	1	1	1	0
5 35 00.4	-5 09 44	12.78 (0.03)	12.42 (0.01)	12.26 (0.01)	11.87 (0.05)	10.98 (0.07)	5.49 (0.06)	0	1	1	0
5 35 21.6	-5 09 38	12.44 (0.02)	10.86 (0.01)	10.10 (0.01)	9.38 (0.01)	8.39 (0.01)	3.98 (0.05)	1	1	0	1
5 35 31.9	-5 09 28	8.03 (0.02)	7.29 (0.01)	6.83 (0.01)	6.40 (0.01)	5.49 (0.01)	2.37 (0.04)	0	1	1	0
5 35 26.8	-5 09 24	11.15 (0.05)	6.81 (0.01)	5.78 (0.01)	4.27 (0.01)	3.34 (0.01)	0.65 (0.25)	1	0	1	0
5 35 21.2	-5 09 16	7.10 (0.03)	6.28 (0.01)	6.01 (0.01)	5.88 (0.01)	5.54 (0.01)	3.96 (0.02)	0	1	1	0
5 35 23.2	-5 08 43	12.98 (0.02)	11.14 (0.01)	10.69 (0.01)	9.91 (0.02)	9.17 (0.04)	5.78 (0.03)	0	0	1	0
5 35 24.3	-5 08 30		11.33 (0.01)	8.91 (0.01)	7.32 (0.01)	5.92 (0.01)	2.20 (0.04)	0	0	0	1
5 35 25.2	-5 08 23		12.71 (0.02)	10.14 (0.01)	8.86 (0.01)	8.13 (0.02)	5.22 (0.03)	0	1	0	1
5 35 23.3	-5 08 21	12.49 (0.03)	10.57 (0.01)	9.79 (0.01)	9.22 (0.01)	8.51 (0.02)	5.61 (0.03)	0	1	1	0
5 35 04.3	-5 08 12	7.27 (0.02)	7.15 (0.01)	7.12 (0.01)	7.09 (0.01)	6.97 (0.01)	6.22 (0.03)	1	1	0	0
5 35 22.4	-5 08 04	8.61 (0.04)	7.25 (0.01)	6.66 (0.01)	6.08 (0.01)	4.98 (0.01)	1.50 (0.06)	0	1	1	0
5 35 38.5	-5 08 03	12.01 (0.02)	10.82 (0.01)	10.25 (0.01)	10.14 (0.01)	9.70 (0.03)	6.24 (0.31)	0	1	1	0
5 35 22.6	-5 08 00	9.21 (0.03)	8.82 (0.01)	8.68 (0.01)	8.26 (0.01)		2.61 (0.04)	1	1	0	0
5 35 25.6	-5 07 57	10.27 (0.06)	9.36 (0.01)	8.52 (0.01)	7.73 (0.01)	6.77 (0.02)	1.46 (0.02)	0	1	0	1
5 35 25.7	-5 07 46	11.23 (0.03)	9.62 (0.01)	8.96 (0.01)	8.40 (0.01)	7.61 (0.03)	3.39 (0.04)	1	0	1	0
5 35 22.3	-5 07 38	10.26 (0.03)	9.04 (0.01)	8.32 (0.01)	7.56 (0.01)	6.54 (0.02)	3.28 (0.02)	1	1	1	0
5 35 44.8	-5 07 17	8.91 (0.02)	8.34 (0.01)	8.27 (0.01)	7.86 (0.01)	6.90 (0.01)	3.16 (0.03)	0	1	1	0
5 35 51.1	-5 07 08	9.87 (0.02)	9.49 (0.01)	9.20 (0.01)	8.85 (0.01)	7.85 (0.01)	4.84 (0.01)	0	1	1	0
5 35 27.7	-5 07 03			12.61 (0.06)			3.96 (0.06)	0	0	0	1
5 35 21.9	-5 07 01	9.32 (0.02)	8.38 (0.01)	7.97 (0.01)	7.72 (0.01)	6.94 (0.03)	3.21 (0.03)	1	1	1	0
5 34 40.6	-5 06 58	11.82 (0.02)	10.88 (0.01)	10.36 (0.01)	10.02 (0.01)	9.47 (0.01)	6.32 (0.03)	1	0	1	0
5 34 45.0	-5 06 49	10.66 (0.02)	9.94 (0.01)	9.79 (0.01)	9.35 (0.01)	8.43 (0.01)	5.22 (0.06)	1	1	1	0
5 35 39.9	-5 06 36	10.80 (0.02)	10.05 (0.01)	9.60 (0.01)	9.20 (0.01)	8.39 (0.01)	5.55 (0.05)	1	1	1	0
5 35 34.3	-5 06 21	9.32 (0.02)	9.36 (0.01)	9.35 (0.01)	9.38 (0.01)	9.32 (0.04)	5.65 (0.04)	0	0	1	0
5 35 24.9	-5 06 21	10.79 (0.02)	9.09 (0.01)	8.30 (0.01)	7.70 (0.01)	6.96 (0.01)	2.59 (0.03)	0	1	0	1
5 34 45.1	-5 06 20	12.23 (0.02)	11.56 (0.01)	11.19 (0.01)	10.88 (0.02)	10.34 (0.04)	7.25 (0.01)	1	0	1	0
5 35 26.7	-5 06 10		12.26 (0.01)	9.87 (0.01)	8.34 (0.01)	7.28 (0.01)	2.88 (0.07)	0	0	0	1
5 35 25.8	-5 05 57	12.65 (0.05)	10.04 (0.01)	8.68 (0.01)	7.85 (0.01)	7.16 (0.01)	4.11 (0.01)	0	0	1	0
5 35 31.5	-5 05 47	8.26 (0.03)	6.47 (0.01)	5.70 (0.01)	4.99 (0.01)	3.98 (0.01)	0.66 (0.01)	1	0	0	1
5 35 28.6	-5 05 44	10.80 (0.02)	9.24 (0.01)	8.66 (0.01)	8.13 (0.01)	7.58 (0.01)	4.34 (0.01)	0	1	1	0
5 35 25.8	-5 05 43			11.85 (0.03)	11.96 (0.09)		4.25 (0.04)	0	0	0	1
5 35 43.6	-5 05 41	10.26 (0.02)	9.31 (0.01)	8.59 (0.01)	8.22 (0.01)	7.35 (0.01)	4.38 (0.13)	1	1	1	0
5 35 27.9	-5 05 36	13.50 (0.04)	11.30 (0.01)	10.55 (0.01)	9.96 (0.02)	9.19 (0.04)	5.39 (0.05)	0	1	0	1

<sup>a</sup> Magnitudes from 2MASS photometry.

<sup>b</sup> From Carpenter, Hillenbrand, & Skrutskie (2001); Those that are variable have Stetson indices greater than 0.55.

Table 3.: Young Stellar Object Candidates in OMC-2/3 detected at 24  $\mu\text{m}$  (continued)

RA J(2000)	Dec J(2000)	$K_S^a$ mag (unc)	3.6 $\mu\text{m}$ mag (unc)	4.5 $\mu\text{m}$ mag (unc)	5.8 $\mu\text{m}$ mag (unc)	8 $\mu\text{m}$ mag (unc)	24 $\mu\text{m}$ mag (unc)	Var.	X-ray	IR-ex <sup>b</sup>	Proto.
5 35 25.2	-5 05 09		12.60 (0.01)	11.09 (0.01)	10.17 (0.01)	9.26 (0.02)	5.73 (0.02)	0	0	0	1
5 35 52.6	-5 05 05	8.75 (0.02)	7.99 (0.01)	7.73 (0.01)	7.52 (0.01)	7.03 (0.01)	3.61 (0.01)	0	1	1	0
5 35 31.5	-5 05 01	10.82 (0.02)	9.89 (0.01)	9.14 (0.01)	8.98 (0.01)	7.93 (0.01)	4.86 (0.04)	1	1	1	0
5 34 49.6	-5 04 59	12.25 (0.02)	11.86 (0.01)	11.61 (0.01)	11.40 (0.02)	10.87 (0.02)	7.94 (0.01)	1	0	1	0
5 35 28.0	-5 04 58			12.20 (0.02)	11.88 (0.05)		5.29 (0.08)	0	0	0	1
5 35 36.2	-5 04 55	10.99 (0.02)	10.28 (0.01)	9.96 (0.01)	9.78 (0.01)	9.16 (0.02)	5.25 (0.01)	1	1	1	0
5 35 19.7	-5 04 54	14.03 (0.04)	10.41 (0.01)	9.01 (0.01)	7.92 (0.01)	6.99 (0.01)	3.35 (0.03)	0	0	0	1
5 34 47.9	-5 04 55	10.62 (0.02)	10.05 (0.01)	9.81 (0.01)	9.64 (0.01)	8.85 (0.01)	4.88 (0.03)	1	1	1	0
5 35 38.5	-5 04 51	12.16 (0.02)	10.47 (0.01)	9.77 (0.01)	9.31 (0.01)	8.29 (0.01)	5.01 (0.02)	0	0	1	0
5 35 08.7	-5 04 40	11.12 (0.02)	10.75 (0.01)	10.37 (0.01)	10.15 (0.01)	9.42 (0.01)	6.76 (0.02)	0	1	1	0
5 34 42.0	-5 04 31	12.61 (0.02)	11.99 (0.01)	11.52 (0.01)	11.22 (0.02)	10.51 (0.02)	7.80 (0.05)	1	0	1	0
5 35 33.8	-5 04 27	10.46 (0.02)	9.11 (0.01)	8.52 (0.01)	8.11 (0.01)	7.44 (0.01)	3.87 (0.02)	1	1	1	0
5 35 54.1	-5 04 14	9.83 (0.03)	9.09 (0.01)	8.71 (0.01)	8.53 (0.01)	8.01 (0.01)	6.20 (0.06)	0	1	1	0
5 35 36.7	-5 04 14	10.77 (0.02)	10.24 (0.01)	9.96 (0.01)	9.76 (0.01)	9.28 (0.02)	5.51 (0.01)	1	1	1	0
5 35 26.6	-5 03 55		8.35 (0.01)	7.07 (0.01)	5.91 (0.01)	4.61 (0.01)	-0.94 (0.02)	0	0	0	1
5 35 18.2	-5 03 54	9.15 (0.02)	9.19 (0.01)	9.15 (0.01)	9.14 (0.01)	8.97 (0.02)	6.28 (0.03)	0	1	0	0
5 35 28.2	-5 03 40	12.50 (0.02)	7.47 (0.01)	6.41 (0.01)	5.11 (0.01)	4.74 (0.01)	0.62 (0.01)	0	1	0	1
5 34 53.0	-5 03 26	10.79 (0.02)	10.18 (0.01)	9.80 (0.01)	9.40 (0.01)	8.65 (0.01)	5.91 (0.05)	1	1	1	0
5 35 43.1	-5 03 07	12.28 (0.02)	11.88 (0.01)	11.60 (0.01)	11.27 (0.02)	10.68 (0.04)	7.32 (0.35)	1	1	1	0
5 35 20.6	-5 03 00	11.83 (0.03)	9.52 (0.01)	8.85 (0.01)	8.25 (0.01)	7.34 (0.01)	3.81 (0.03)	1	0	1	0
5 35 15.3	-5 02 50	14.19 (0.05)	12.91 (0.02)	12.43 (0.02)	11.88 (0.04)	11.00 (0.05)	8.34 (0.04)	0	0	1	0
5 35 27.4	-5 02 42	10.98 (0.02)	9.28 (0.01)	8.66 (0.01)	8.18 (0.01)	7.65 (0.01)	4.83 (0.03)	1	1	1	0
5 35 37.3	-5 02 36	12.07 (0.02)	10.76 (0.01)	10.18 (0.01)	10.03 (0.01)	9.47 (0.02)	6.28 (0.01)	1	0	1	0
5 35 14.7	-5 02 27	11.55 (0.05)	10.63 (0.01)	10.39 (0.01)	10.06 (0.01)	9.80 (0.02)	6.67 (0.06)	0	0	1	0
5 35 32.5	-5 01 57	12.75 (0.03)	11.92 (0.01)	11.58 (0.01)	10.93 (0.03)	9.81 (0.05)	6.93 (0.01)	0	0	1	0
5 35 23.6	-5 01 40	15.50 (0.15)	11.76 (0.01)	10.12 (0.01)	8.20 (0.01)	6.99 (0.01)	1.75 (0.01)	0	0	0	1
5 35 28.0	-5 01 34	12.50 (0.02)	10.23 (0.01)	9.43 (0.01)	8.94 (0.01)	8.32 (0.01)	5.58 (0.01)	1	1	1	0
5 35 48.4	-5 01 28	10.53 (0.02)	9.50 (0.01)	9.05 (0.01)	8.81 (0.01)	8.11 (0.01)	4.35 (0.01)	1	1	1	0
5 35 23.5	-5 01 28		13.97 (0.02)	11.19 (0.01)	10.42 (0.01)	9.20 (0.02)	2.44 (0.20)	0	0	0	1
5 35 21.5	-5 01 15	13.28 (0.08)	12.46 (0.01)	10.06 (0.01)	10.63 (0.02)	10.49 (0.09)	6.11 (0.03)	0	0	1	0
5 35 36.4	-5 01 15	9.13 (0.02)	8.59 (0.01)	8.32 (0.01)	8.02 (0.01)	7.44 (0.01)	5.09 (0.02)	1	1	1	0
5 35 22.4	-5 01 14		16.22 (0.09)	12.77 (0.02)	12.04 (0.04)	11.88 (0.11)	3.23 (0.05)	0	0	0	1
5 34 56.5	-5 01 06	13.05 (0.03)	12.66 (0.01)	12.22 (0.01)	11.72 (0.03)	10.77 (0.04)	7.38 (0.06)	0	0	1	0
5 35 20.0	-5 01 02	14.47 (0.06)	10.16 (0.01)	8.82 (0.01)	7.78 (0.01)	7.35 (0.01)	3.75 (0.02)	0	1	0	1
5 35 34.5	-5 00 52	11.48 (0.03)	8.24 (0.01)	7.12 (0.01)	6.29 (0.01)	5.47 (0.01)	1.80 (0.04)	0	0	0	1
5 35 18.9	-5 00 50			12.58 (0.07)	10.16 (0.03)	8.76 (0.01)	4.06 (0.01)	0	0	0	1

<sup>a</sup> Magnitudes from 2MASS photometry.

<sup>b</sup> From Carpenter, Hillenbrand, & Skrutskie (2001); Those that are variable have Stetson indices greater than 0.55.

Table 3.: Young Stellar Object Candidates in OMC-2/3 detected at 24  $\mu\text{m}$  (continued)

RA J(2000)	Dec J(2000)	$K_S^a$ mag (unc)	3.6 $\mu\text{m}$ mag (unc)	4.5 $\mu\text{m}$ mag (unc)	5.8 $\mu\text{m}$ mag (unc)	8 $\mu\text{m}$ mag (unc)	24 $\mu\text{m}$ mag (unc)	Var.	X-ray	IR-ex <sup>b</sup>	Proto.
5 35 18.3	-5 00 32	11.07 (0.04)	7.41 (0.01)	5.97 (0.01)	5.07 (0.01)	4.24 (0.01)	0.44 (0.01)	0	0	0	1
5 35 13.0	-5 00 26	14.81 (0.08)	13.11 (0.01)	12.53 (0.02)	12.16 (0.05)	12.05 (0.09)	6.83 (0.01)	0	1	1	0
5 35 31.6	-5 00 14	10.13 (0.02)	8.17 (0.01)	7.71 (0.01)	7.19 (0.01)	6.78 (0.01)	4.28 (0.03)	1	1	1	0
5 35 15.0	-5 00 08	14.66 (0.14)	12.86 (0.01)	11.66 (0.01)	11.03 (0.03)	10.50 (0.04)	4.26 (0.02)	0	0	0	1
5 35 16.2	-5 00 02	11.98 (0.04)	9.35 (0.01)	8.26 (0.01)	7.42 (0.01)	6.55 (0.01)	1.29 (0.01)	0	0	0	1
5 35 34.2	-4 59 52		14.13 (0.04)	12.39 (0.02)	11.13 (0.04)	10.60 (0.08)	5.14 (0.02)	0	1	0	1
5 35 26.5	-4 59 52	12.90 (0.03)	11.35 (0.01)	11.05 (0.01)	10.38 (0.02)	9.77 (0.03)	6.78 (0.03)	1	1	1	0
5 35 38.5	-4 59 41	10.35 (0.02)	9.77 (0.01)	9.39 (0.01)	9.17 (0.01)	8.38 (0.02)	5.50 (0.01)	1	1	1	0
5 35 30.6	-4 59 35	10.35 (0.02)	9.06 (0.01)	8.50 (0.01)	8.14 (0.01)	7.36 (0.01)	3.62 (0.05)	1	1	1	0
5 35 15.6	-4 59 27	11.51 (0.02)	10.29 (0.01)	9.77 (0.01)	9.16 (0.04)	8.12 (0.07)	4.39 (0.05)	0	1	1	0
5 35 29.7	-4 58 48			13.73 (0.06)	11.00 (0.03)	9.55 (0.03)	4.21 (0.07)	0	0	0	1
5 35 10.5	-4 58 45	10.57 (0.02)	7.24 (0.01)	6.24 (0.01)	5.57 (0.01)	4.98 (0.01)	2.59 (0.14)	0	1	1	0
5 35 28.2	-4 58 38	11.57 (0.03)	9.13 (0.01)	8.24 (0.01)	7.46 (0.01)	6.85 (0.01)	4.88 (0.06)	1	1	1	0
5 34 50.7	-4 58 36	10.74 (0.02)	10.15 (0.01)	9.92 (0.01)	9.66 (0.01)	9.21 (0.01)	7.37 (0.01)	1	0	1	0
5 35 04.6	-4 58 28	11.09 (0.02)	9.97 (0.01)	9.62 (0.01)	9.33 (0.01)	8.68 (0.01)	5.53 (0.04)	1	1	1	0
5 35 54.8	-4 58 19	12.66 (0.03)	11.75 (0.01)	11.26 (0.01)	10.62 (0.02)	9.55 (0.02)	5.75 (0.08)	1	0	1	0
5 34 40.5	-4 57 39	11.75 (0.02)	11.21 (0.01)	10.95 (0.01)	10.86 (0.02)	10.19 (0.02)	6.40 (0.01)	1	0	1	0
5 34 53.4	-4 57 32	12.27 (0.02)	11.83 (0.01)	11.49 (0.01)	11.10 (0.02)	10.45 (0.03)	7.70 (0.03)	0	0	1	0
5 34 57.7	-4 57 19	13.02 (0.03)	11.40 (0.01)	10.78 (0.01)	10.28 (0.02)	9.72 (0.03)	5.79 (0.05)	0	0	1	0
5 35 09.5	-4 57 11	12.71 (0.02)	12.12 (0.01)	11.33 (0.01)	10.83 (0.05)	9.61 (0.08)	6.34 (0.02)	1	0	0	1

<sup>a</sup> Magnitudes from 2MASS photometry.

<sup>b</sup> From Carpenter, Hillenbrand, & Skrutskie (2001); Those that are variable have Stetson indices greater than 0.55.

Table 4. Young Brown Dwarfs in OMC-2/3<sup>k</sup>

Name	RA <sup>a</sup> (J2000)	Dec. <sup>a</sup> (J2000)	I, $\sigma_I^b$ (mag)	J, $\sigma_J^c$ (mag)	H, $\sigma_H^c$ (mag)	K, $\sigma_K^c$ (mag)	Spectral Type	A <sub>H</sub> <sup>i</sup>	EW[H $\alpha$ ] (Å)
1	05 35 27.4	-05 09 04	17.882 ± 0.036	14.852 ± 0.009	14.107 ± 0.008	13.594 ± 0.011	M6.5 <sup>d</sup>	0.2	-19.2
2	05 35 16.8	-05 07 27	17.819 ± 0.018	14.953 ± 0.009	14.413 ± 0.009	13.947 ± 0.011	M6.5 <sup>d</sup>	0.0	-16.9
3	05 35 13.0	-05 02 09	17.393 ± 0.005	14.465 ± 0.007	13.895 ± 0.007	13.477 ± 0.007	M6.5 <sup>d</sup>	0.0	-25.8
29	05 35 12.9	-05 15 49	18.447 ± 0.051	15.082 ± 0.015	14.309 ± 0.013	13.806 ± 0.015	M8-M8.25 <sup>e</sup> M8.5 <sup>g</sup>	0.2	neb <sup>j</sup>
30	05 35 12.7	-05 15 43	18.394 ± 0.069	14.825 ± 0.010	13.951 ± 0.010	13.328 ± 0.008	M7 <sup>e</sup> M7.25 <sup>g</sup>	0.4	neb <sup>j</sup>
31	05 35 18.7	-05 15 18	18.003 ± 0.062	14.488 ± 0.009	13.658 ± 0.007	13.077 ± 0.009	M7.75 <sup>e</sup> M7.5 <sup>h</sup>	0.3	neb <sup>j</sup>
21	05 35 38.2	-05 03 34	18.561 ± 0.018	16.112 ± 0.027	15.373 ± 0.031	14.840 ± 0.024	M7 <sup>f</sup> M7.25 <sup>h</sup>	0.2	-105.1
34	05 35 13.6	-05 14 22	18.445 ± 0.077	15.793 ± 0.020	14.880 ± 0.017	14.335 ± 0.022	M8 <sup>f</sup>	0.4	
77	05 35 40.3	-05 12 32	19.290 ± 0.40?	15.462 ± 0.026	14.687 ± 0.018	14.155 ± 0.019	M7 <sup>f</sup>	0.2	
923_1621	05 35 15.1	-04 58 09		17.867 ± 0.051	16.197 ± 0.028	15.200 ± 0.029	M8 <sup>g</sup>	1.5	
1036_108	05 35 10.1	-05 14 56		16.551 ± 0.032	15.397 ± 0.022	14.594 ± 0.020	M9 <sup>g</sup>	0.8	
543_681	05 35 32.0	-05 08 35		16.848 ± 0.026	15.430 ± 0.017	14.485 ± 0.014	M7.25 <sup>g</sup>	1.2	
766_341	05 35 22.1	-05 12 21		17.035 ± 0.081	15.908 ± 0.040	14.873 ± 0.027	M7.75 <sup>g</sup>	0.7	
441_326	05 35 36.6	-05 12 31		16.547 ± 0.070	15.758 ± 0.058	14.906 ± 0.051	M8.5 <sup>g</sup>	0.3	
988_148	05 35 12.2	-05 14 29		17.851 ± 0.069	16.503 ± 0.037	15.304 ± 0.030	M8 <sup>g</sup>	1.1	
1004_979	05 35 11.5	-05 05 16		16.321 ± 0.019	14.986 ± 0.011	14.330 ± 0.011	M7 <sup>g</sup>	1.0	
727_1506	05 35 23.9	-04 59 25		18.398 ± 0.070	16.800 ± 0.034	15.842 ± 0.031	M7.75 <sup>g</sup>	1.4	
845_236	05 35 23.3	-05 13 48		16.714 ± 0.060	15.789 ± 0.037	14.607 ± 0.029	M7 <sup>g</sup>	0.5	
735_36	05 35 28.2	-05 16 01		15.790 ± 0.049	14.673 ± 0.020	13.978 ± 0.021	M8-M8.25 <sup>g</sup>	0.7	

<sup>a</sup> Coordinates from 2MASS final release.

<sup>b</sup> Magnitudes from 4-Shooter photometry.

<sup>c</sup> Magnitudes from SQIID photometry.

<sup>d</sup> Keck LRIS spectra.

<sup>e</sup> Blue Channel MMT spectra.

<sup>f</sup> Red Channel MMT spectra.

<sup>g</sup> SpeX IRTF spectra.

<sup>h</sup> CorMASS spectra.

<sup>i</sup> A<sub>H</sub> values calculated from J - H colors and not from the A<sub>V</sub> values found as the best fit from spectral classification.

<sup>j</sup> Too much emission from surrounding H II region to measure H $\alpha$ .

<sup>k</sup> Table from Peterson et al. (2008).

#### 4. The NGC 1977 Region

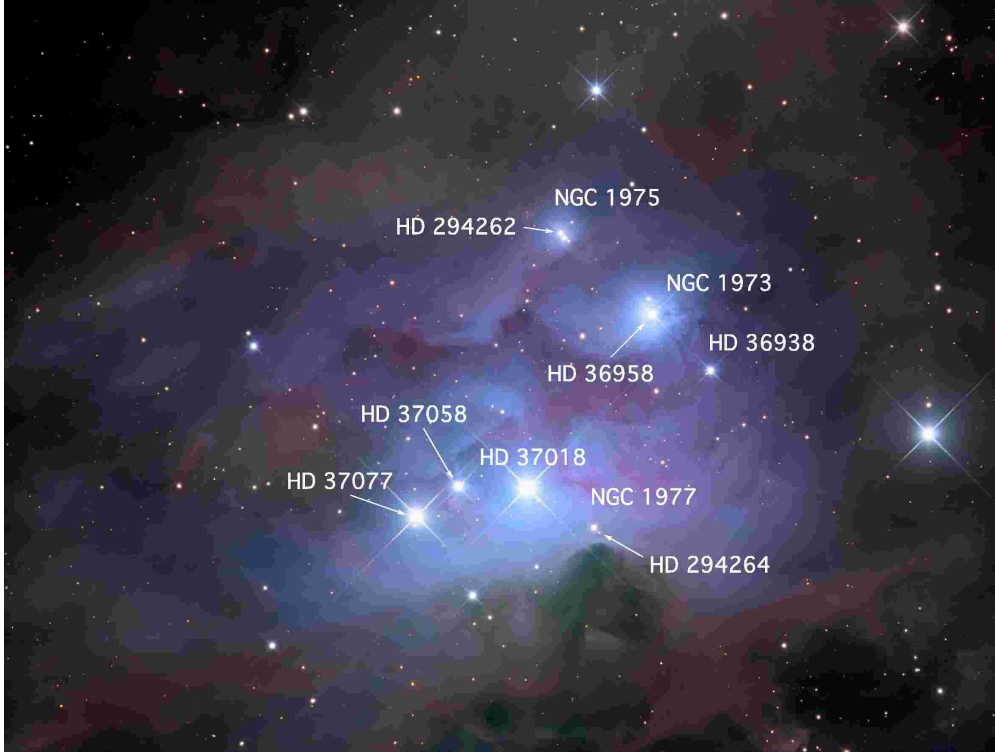


Figure 11. The NGC 1977 HII region is primarily excited by the B1 V star HD 37018. NGC 1973 and NGC 1975 are smaller nebulae, but often the designation NGC 1977 is used for the whole region. The field is approximately  $30 \times 45$  arcmin, with north up and east left. Image courtesy Martin Pugh.

The NGC 1977 nebula north of the Orion Nebula was discovered by William Herschel in 1786, while the two smaller regions NGC 1973 and 1975 were noted by Heinrich Louis d'Arrest in 1862 and 1864, respectively, see Figure 11. The designation NGC 1977 is often used for the whole complex. NGC 1977 comprises the southern portion of the H II region S279, at the northern end of the Orion molecular cloud, defining an interface between the H II region and dense molecular cloud (Kutner, Evans, & Tucker 1976). The ionizing source for the H II region is the B1 V star HD 37018 (42 Ori) (Sharpless 1959; Johnson et al. 1977). In Figures 11 and 12, HD 37018 appears as the brightest star near the middle of the image. There are two B3 V stars that flank the east (HD 37058) and south-west (HD 294264) sides of HD 37018; the other star to the east of HD 37018, which appears almost as bright, is HD 37077 (45 Ori), a F0 III star. The star of approximately equal brightness to the north-west is HD 36958 (KX Ori), yet another B3 V star, which illuminates NGC 1973. Further to the northeast is HD 294262, an A0 double star (the companion is LZ Ori, also an A0 star), which illuminates NGC 1975.

Just south of the B3 V star HD 37058 is HH 45, the most prominent HH object in NGC 1977. It was first discovered by Schwartz (1977), and is discussed in detail in

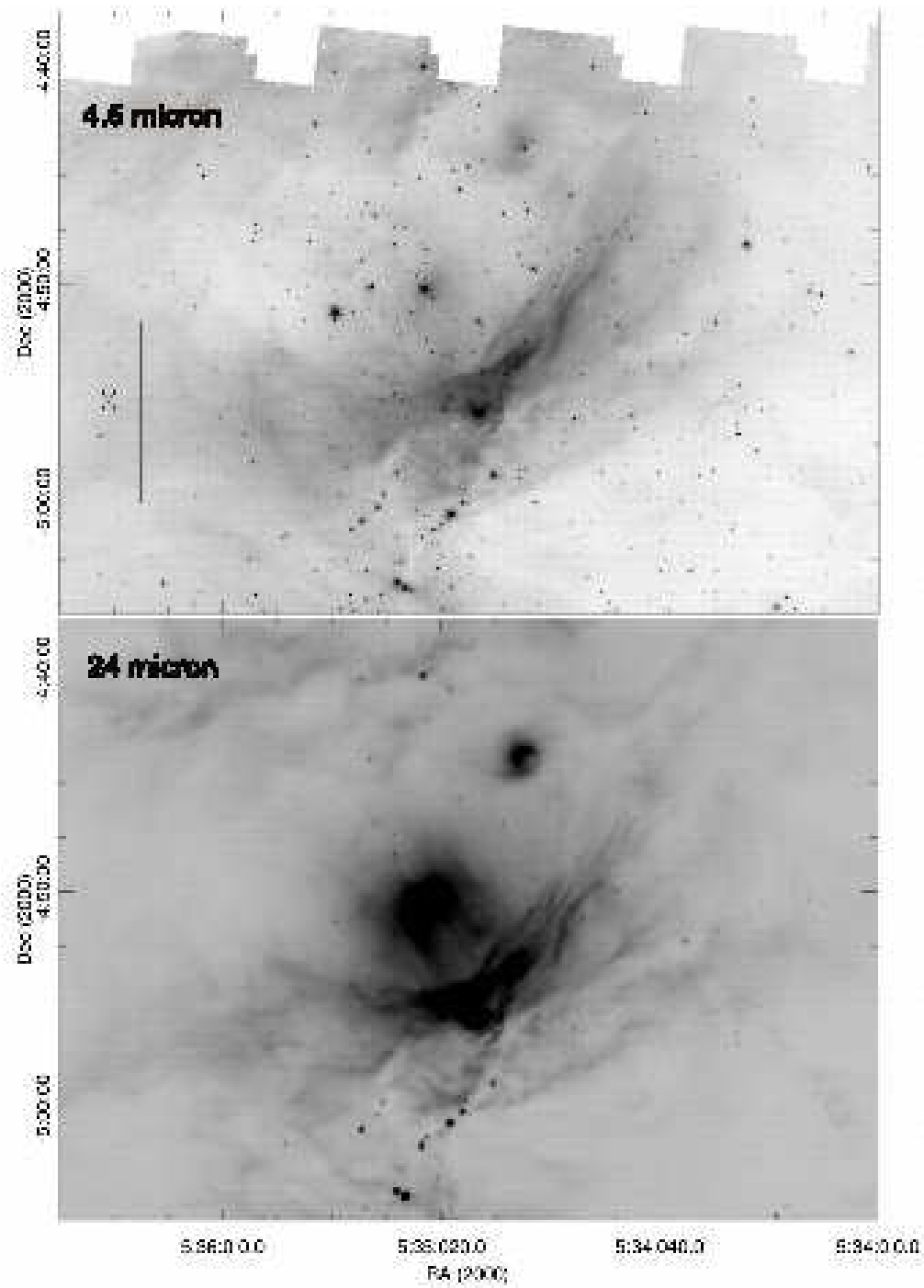


Figure 12. NGC 1977 as seen at the *Spitzer* 4.5 and 24  $\mu\text{m}$  wavelengths (Megeath et al. 2008a, in prep). The bright star in the center is the B1V star HD 37018. Bright nebulosity is seen surrounding the star, particularly at 24  $\mu\text{m}$ , as well as south of this star at the edge of the molecular filament. Within this filament, protostars in the OMC-3 region can be found (see Figure 13).

Reipurth (1989). The object has a bow-shock shape: the eastern side of the bow-shock has a well defined boundary while the western side is more extended. The bow-shock has several bright knots, and an additional knot is visible to the south of the bow-shock; these are shown in Figure 9b of Reipurth (1989). The source for HH 45 is not known. To the south-west of HH 45, Stanke, McCaughrean, & Zinnecker (2002) detected two knots of  $2.12 \mu\text{m}$   $\text{H}_2$  emission on either side of a near-infrared source; they refer to this source as SMZ 1.

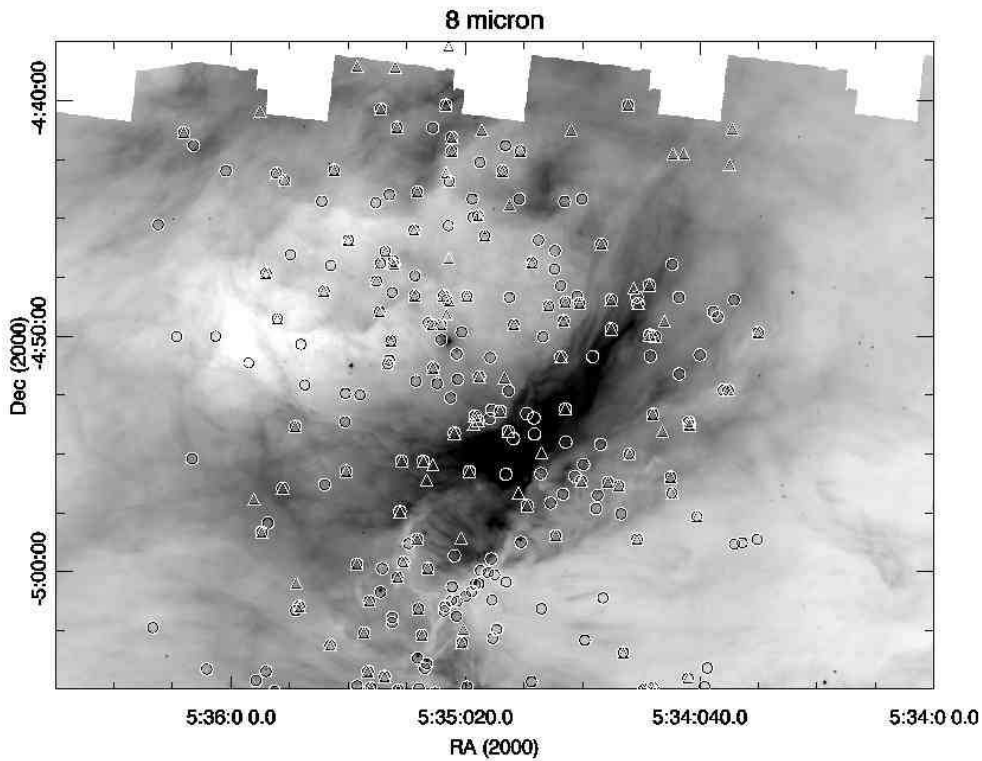


Figure 13. NGC 1977 as seen with *Spitzer* at  $8 \mu\text{m}$  (Megeath et al. 2008a, in prep). The bright star in the center is the B1V star HD 37018. The positions of young stars and protostars are plotted: the triangles are variables from Carpenter, Hillenbrand, & Skrutskie (2001), and the circles are infrared excess sources from Megeath et al. (2008a, in prep). A total of 170 young stellar objects are found with either infrared excess or variability.

The *Spitzer* observations show that the H II region fills a loop of  $8 \mu\text{m}$  emission (Figure 13). This suggests that NGC 1977 is part of a larger cavity excavated in the molecular gas by the B stars and that the H II region is gas ionized off the cavity by the B stars. The  $8 \mu\text{m}$  emission is brightest toward NGC 1977, where the loop intersects the filament of dense molecular gas and the OMC-2/3 region. Makinen et al. (1985) find that this region is externally heated by HD 37018, and the radio continuum observations presented in their paper rule out the possibility of additional heating by any embedded stars earlier than B2.5-B3. Detailed observations of the interface between NGC 1977

and the molecular cloud to the south by Kutner et al. (1985) show that the density of the molecular cloud drops off gradually toward the interface.

The distribution of young stars in Figure 13 shows a concentration of stars within the loop. These are presumably the young, low mass stars associated with the B stars. The *Spitzer* observations show 146 stars within NGC 1977 with infrared excesses, as selected by the color-color diagrams in Figure 9. Of the 146 stars with infrared excesses, six appear to be protostars (Class 0/I) based on their 3.6–4.5 and 4.5–24  $\mu\text{m}$  colors (Megeath et al. 2008a, in prep). The remaining 140 infrared excess sources are primarily young stars with disks (Class II), although some protostars that were not detected at 24  $\mu\text{m}$  may be among the 140 sources. In addition, Carpenter, Hillenbrand, & Skrutskie (2001) identified 97 variables in the same region; 24 of the variables do not have infrared excesses (Class III). In total, there are 170 young stellar objects in NGC 1977 identified by the presence of an infrared excess or variability (note that there is no Chandra data toward NGC 1977 so X-rays were not used for pre-main sequence star selection). The positional limits used for this analysis are  $\alpha = 05^{\text{h}} 34^{\text{m}} 30^{\text{s}}$  to  $05^{\text{h}} 36^{\text{m}} 15^{\text{s}}$ ,  $\delta = -04^{\circ} 57' 00''$  to  $-04^{\circ} 37' 30''$  (J2000). The photometry for the young stellar objects in NGC 1977 with *Spitzer* 24  $\mu\text{m}$  detections is presented in Table 5.

## 5. Summary

The northern end of the Orion A molecular cloud is the most active region of low and high mass star formation within 500 pc of our Sun and is one of the most intensively studied star forming regions in the sky. However, most of these observations exclusively target the Orion Nebula and the region immediately surrounding the nebula. This chapter reviews the rich concentration of pre-main sequence stars and protostars north of the Orion Nebula in OMC-2/3 and NGC 1977. These regions provide examples of star formation in environments much different than that in the Orion Nebula; in particular, in environments without the extreme-UV radiation found in the Orion Nebula, and showing lower stellar densities than the densities found in the center of the Orion Nebula. Future studies of the ONC should encompass OMC-2/3 and NGC 1977 in order to fully characterize the wide variety of environments within this single contiguous star forming region and how these environments affect star and planet formation.

**Acknowledgments.** We would like to thank Chris Davis for Figure 6 and for input into Section 3.3., Nick Siegler for providing the *Spitzer* 24  $\mu\text{m}$  photometry, and Martin Pugh for the color image of NGC 1977. The initial work on this chapter was done while co-author Peterson was at the University of Virginia and while co-author Megeath was at the Harvard-Smithsonian Center for Astrophysics. Support for Megeath’s work at that time was provided by NASA through contract 1256970 issued by Jet Propulsion Laboratory (JPL)/Caltech. This work includes observations made with the *Spitzer* Space Telescope, which is operated by JPL/Caltech under NASA contract 1407. This publication makes use of data products from the Two-Micron All Sky Survey, which is a joint project of the University of Massachusetts and the Infrared Processing and Analysis Center (IPAC)/Caltech, funded by NASA and the NSF. This research has made use of the NASA/IPAC Infrared Science Archive, which is operated by JPL and Caltech under contract with NASA, of the SIMBAD database, operated at CDS, Strasbourg, France, and of NASA’s Astrophysics Data System Bibliographic Services.

Table 5.: Young Stellar Object Candidates in NGC 1977 detected at 24  $\mu\text{m}$ 

RA J(2000)	Dec J(2000)	$K_S^a$ mag (unc)	3.6 $\mu\text{m}$ mag (unc)	4.5 $\mu\text{m}$ mag (unc)	5.8 $\mu\text{m}$ mag (unc)	8 $\mu\text{m}$ mag (unc)	24 $\mu\text{m}$ mag (unc)	Var.	IR-ex <sup>b</sup>	Proto.
5 34 57.4	-4 56 45	11.63 (0.02)	10.42 (0.01)	9.81 (0.01)	9.23 (0.01)	8.16 (0.01)	5.73 (0.02)	0	1	0
5 35 03.3	-4 56 42	11.31 (0.02)	10.92 (0.01)	10.57 (0.01)	10.34 (0.03)	9.47 (0.04)	5.83 (0.02)	0	1	0
5 34 44.8	-4 56 40	12.23 (0.02)	11.65 (0.01)	11.11 (0.01)	10.89 (0.02)	10.38 (0.05)	7.53 (0.08)	1	1	0
5 35 51.2	-4 56 27	11.54 (0.02)	11.14 (0.01)	10.50 (0.01)	9.81 (0.02)	8.66 (0.03)	4.81 (0.08)	1	1	0
5 34 53.9	-4 56 22	10.91 (0.02)	10.22 (0.01)	10.33 (0.01)	9.81 (0.01)	9.36 (0.02)	4.87 (0.01)	1	1	0
5 34 55.7	-4 56 12	10.22 (0.02)	9.22 (0.01)	8.83 (0.01)	8.50 (0.01)	7.79 (0.01)	4.71 (0.04)	1	1	0
5 35 00.3	-4 56 08	12.57 (0.02)	11.81 (0.01)	11.48 (0.01)	11.19 (0.04)	10.51 (0.07)	6.78 (0.01)	1	1	0
5 34 45.0	-4 55 59	11.35 (0.03)	10.18 (0.01)	9.78 (0.01)	9.53 (0.01)	8.96 (0.03)	5.61 (0.05)	1	1	0
5 35 19.3	-4 55 44	10.08 (0.02)	8.28 (0.01)	7.27 (0.01)	6.70 (0.01)	5.94 (0.01)	2.66 (0.06)	1	1	0
5 35 40.4	-4 55 44	12.20 (0.02)	11.70 (0.01)	11.55 (0.01)	11.42 (0.03)	10.66 (0.04)	6.35 (0.08)	1	1	0
5 35 30.9	-4 55 17	10.67 (0.02)	10.13 (0.01)	9.75 (0.01)	9.41 (0.02)	8.36 (0.03)	4.72 (0.17)	1	1	0
5 34 52.0	-4 55 00	11.69 (0.02)	10.89 (0.01)	10.47 (0.01)	10.18 (0.02)	9.14 (0.02)	5.49 (0.06)	1	1	0
5 35 08.2	-4 54 09	10.15 (0.02)	8.16 (0.01)	7.36 (0.01)	6.43 (0.01)	5.06 (0.01)	2.48 (0.03)	0	0	1
5 34 41.8	-4 53 46	11.03 (0.02)	10.54 (0.01)	10.24 (0.01)	9.95 (0.02)	8.98 (0.02)	5.40 (0.02)	1	1	0
5 35 40.5	-4 53 37		15.13 (0.07)	14.98 (0.09)	12.16 (0.09)	10.32 (0.09)	6.42 (0.10)	0	1	0
5 35 15.9	-4 53 29	13.52 (0.03)	12.52 (0.01)	12.10 (0.02)	11.56 (0.08)		6.00 (0.03)	0	1	0
5 35 18.4	-4 53 23	10.11 (0.02)	9.01 (0.01)	8.47 (0.01)	8.09 (0.01)	7.28 (0.01)	4.19 (0.01)	1	1	0
5 35 14.1	-4 53 11	12.34 (0.02)	10.65 (0.01)	10.10 (0.01)	9.56 (0.01)	8.82 (0.01)	4.82 (0.04)	1	1	0
5 35 22.5	-4 52 36	10.68 (0.02)	9.72 (0.01)	9.09 (0.01)	8.44 (0.01)	7.24 (0.01)	4.15 (0.19)	0	1	0
5 35 40.5	-4 52 26	11.62 (0.02)	11.25 (0.01)	10.98 (0.01)	10.79 (0.02)	10.14 (0.02)	7.38 (0.02)	0	1	0
5 34 35.2	-4 52 17	11.80 (0.02)	10.66 (0.01)	9.85 (0.01)	9.04 (0.01)	7.92 (0.01)	3.66 (0.01)	1	0	1
5 35 47.4	-4 52 04	15.04 (0.10)	14.35 (0.03)	13.75 (0.03)	13.24 (0.09)	12.34 (0.08)	7.85 (0.04)	0	1	0
5 35 13.3	-4 51 44	7.58 (0.03)	7.47 (0.01)	7.42 (0.01)	7.40 (0.01)	7.36 (0.01)	4.42 (0.05)	1	0	0
5 34 43.5	-4 51 36	11.77 (0.02)	11.64 (0.01)	11.59 (0.01)	11.34 (0.05)	10.77 (0.12)	6.37 (0.02)	0	1	0
5 35 25.5	-4 51 20	10.69 (0.02)	9.98 (0.01)	9.45 (0.01)	9.25 (0.01)	8.20 (0.01)	4.75 (0.05)	1	1	0
5 35 03.7	-4 50 52	9.60 (0.02)	8.92 (0.01)	8.41 (0.01)	8.12 (0.01)	7.25 (0.02)	3.75 (0.02)	1	1	0
5 34 48.4	-4 50 51	12.38 (0.02)	11.81 (0.01)	11.36 (0.01)	11.02 (0.03)	10.14 (0.05)	6.53 (0.05)	0	1	0
5 35 21.5	-4 50 45	8.94 (0.02)	8.30 (0.01)	8.08 (0.01)	7.83 (0.01)	7.11 (0.01)	2.78 (0.02)	0	1	0
5 35 48.1	-4 50 20	12.30 (0.02)	11.87 (0.01)	11.69 (0.01)	11.50 (0.03)	10.93 (0.03)	7.25 (0.04)	0	1	0
5 35 32.7	-4 50 11	9.62 (0.03)	8.73 (0.01)	8.30 (0.01)	7.99 (0.01)	7.33 (0.01)	4.69 (0.06)	1	1	0
5 36 09.3	-4 50 00	11.80 (0.02)	11.23 (0.01)	10.94 (0.01)	10.72 (0.02)	10.00 (0.01)	7.24 (0.04)	0	1	0
5 35 06.8	-4 50 01	15.40 (0.16)	14.51 (0.03)	13.65 (0.03)	12.63 (0.06)	10.94 (0.05)	6.73 (0.01)	0	0	1
5 34 47.6	-4 50 01	10.95 (0.02)	10.58 (0.01)	10.47 (0.01)	10.38 (0.03)	9.37 (0.03)	4.23 (0.15)	1	1	0
5 34 48.5	-4 49 56	11.16 (0.02)	9.91 (0.01)	9.30 (0.01)	9.36 (0.02)	8.58 (0.04)	5.30 (0.03)	1	1	0
5 34 30.1	-4 49 50	10.96 (0.02)	10.51 (0.01)	10.33 (0.01)	10.31 (0.02)	10.06 (0.02)	6.34 (0.01)	1	1	0

<sup>a</sup> Magnitudes from 2MASS photometry.

<sup>b</sup> From Carpenter, Hillenbrand, & Skrutskie (2001); Those that are variable have Stetson indices greater than 0.55.

Table 5.: Young Stellar Object Candidates in NGC 1977 detected at 24  $\mu\text{m}$  (continued)

RA J(2000)	Dec J(2000)	$K_S^a$ mag (unc)	3.6 $\mu\text{m}$ mag (unc)	4.5 $\mu\text{m}$ mag (unc)	5.8 $\mu\text{m}$ mag (unc)	8 $\mu\text{m}$ mag (unc)	24 $\mu\text{m}$ mag (unc)	Var.	IR-ex <sup>b</sup>	Proto.
5 35 11.8	-4 49 30	12.11 (0.02)	11.02 (0.01)	10.50 (0.01)	10.09 (0.01)	9.28 (0.01)	5.44 (0.06)	1	1	0
5 35 03.2	-4 49 20	8.51 (0.02)	7.68 (0.01)	7.25 (0.01)	7.08 (0.01)	6.59 (0.01)	3.86 (0.02)	1	1	0
5 35 52.1	-4 49 15	12.61 (0.02)	11.97 (0.01)	11.48 (0.01)	11.31 (0.03)	10.61 (0.02)	8.33 (0.03)	1	1	0
5 34 37.0	-4 49 10	12.89 (0.02)	11.94 (0.01)	11.63 (0.01)	11.44 (0.03)	10.92 (0.06)	7.70 (0.06)	0	1	0
5 35 34.6	-4 48 57	12.58 (0.03)	10.73 (0.01)	10.12 (0.01)	9.35 (0.01)	8.40 (0.01)	5.54 (0.02)	1	1	0
5 34 37.7	-4 48 57	11.91 (0.02)	11.75 (0.01)	11.70 (0.01)	11.65 (0.03)	11.34 (0.06)	6.56 (0.07)	0	1	0
5 35 05.8	-4 48 42	10.57 (0.02)	9.88 (0.01)	9.52 (0.01)	9.37 (0.01)	8.62 (0.01)	5.88 (0.03)	1	1	0
5 34 50.6	-4 48 37	12.64 (0.02)	11.49 (0.01)	10.95 (0.01)	10.58 (0.03)	9.77 (0.06)	6.60 (0.29)	1	1	0
5 35 00.5	-4 48 35	12.37 (0.02)	11.23 (0.01)	10.64 (0.01)	10.19 (0.02)	9.35 (0.03)	6.39 (0.02)	1	1	0
5 35 03.0	-4 48 32	12.19 (0.03)	11.78 (0.01)	11.54 (0.01)	11.18 (0.03)	10.02 (0.03)	6.88 (0.01)	1	1	0
5 34 34.2	-4 48 27	11.71 (0.02)	11.40 (0.01)	11.23 (0.01)	11.03 (0.03)	10.21 (0.05)	6.54 (0.01)	0	1	0
5 35 23.2	-4 48 27	14.50 (0.09)	13.18 (0.02)	12.77 (0.02)	12.26 (0.05)	10.89 (0.04)	5.47 (0.07)	0	1	0
5 34 55.1	-4 48 27	10.17 (0.02)	10.08 (0.01)	10.07 (0.01)	10.04 (0.02)	9.92 (0.09)	4.47 (0.03)	1	1	0
5 35 00.9	-4 48 18	11.26 (0.02)	10.79 (0.01)	10.50 (0.01)	10.19 (0.02)	9.37 (0.02)	6.98 (0.01)	0	1	0
5 35 23.7	-4 48 16	12.02 (0.02)	11.53 (0.01)	11.10 (0.01)	10.60 (0.01)	9.33 (0.01)	6.07 (0.01)	1	1	0
5 35 28.7	-4 48 16	12.88 (0.02)	9.40 (0.01)	8.65 (0.01)	7.93 (0.01)	7.13 (0.01)	3.87 (0.02)	1	1	0
5 35 44.1	-4 48 04	10.72 (0.02)	10.01 (0.01)	9.70 (0.01)	9.58 (0.01)	9.04 (0.01)	5.75 (0.03)	1	1	0
5 34 48.6	-4 47 50	11.94 (0.02)	11.47 (0.01)	10.95 (0.01)	10.86 (0.03)	10.07 (0.03)	6.51 (0.02)	1	1	0
5 35 35.2	-4 47 39	11.26 (0.02)	10.80 (0.01)	10.52 (0.01)	10.17 (0.02)	8.81 (0.01)	4.49 (0.01)	1	1	0
5 35 28.6	-4 47 26	11.20 (0.02)	10.63 (0.01)	10.25 (0.01)	9.91 (0.01)	9.03 (0.02)	5.95 (0.07)	0	1	0
5 35 54.1	-4 47 19	11.04 (0.02)	10.05 (0.01)	9.60 (0.01)	9.23 (0.01)	8.63 (0.01)	5.65 (0.02)	1	1	0
5 35 43.0	-4 47 00	12.18 (0.02)	11.87 (0.01)	11.66 (0.01)	11.39 (0.03)	10.74 (0.04)	8.32 (0.11)	0	1	0
5 35 32.2	-4 46 57	10.17 (0.02)	9.41 (0.01)	9.00 (0.01)	8.62 (0.01)	7.66 (0.01)	4.72 (0.01)	1	1	0
5 35 34.5	-4 46 54	11.01 (0.02)	10.67 (0.01)	10.22 (0.01)	9.66 (0.01)	8.64 (0.01)	5.71 (0.04)	1	1	0
5 35 08.7	-4 46 52	9.91 (0.02)	8.64 (0.01)	8.28 (0.01)	7.73 (0.01)	7.04 (0.01)	4.23 (0.01)	1	1	0
5 35 32.3	-4 46 48	13.57 (0.06)	11.66 (0.01)	10.84 (0.01)	10.15 (0.02)	9.31 (0.02)	5.30 (0.08)	1	0	1
5 35 22.8	-4 46 41	11.80 (0.02)	11.23 (0.01)	11.02 (0.01)	10.68 (0.02)	10.11 (0.02)	6.93 (0.30)	1	0	0
5 35 49.9	-4 46 32	11.46 (0.02)	11.06 (0.01)	10.75 (0.01)	10.41 (0.02)	9.68 (0.03)	6.63 (0.01)	0	1	0
5 35 33.7	-4 46 23	10.84 (0.02)	10.47 (0.01)	10.35 (0.01)	10.23 (0.02)	9.67 (0.02)	5.33 (0.07)	1	1	0
5 35 04.7	-4 46 21	13.38 (0.03)	12.96 (0.02)	12.51 (0.02)	12.10 (0.05)	11.51 (0.08)	7.82 (0.07)	0	1	0
5 34 56.8	-4 46 04	10.96 (0.02)	9.94 (0.01)	9.64 (0.01)	9.25 (0.01)	9.00 (0.02)	6.54 (0.02)	1	1	0
5 35 40.0	-4 45 54	10.42 (0.02)	10.03 (0.01)	9.79 (0.01)	9.48 (0.01)	8.62 (0.01)	6.02 (0.01)	1	1	0
5 35 16.7	-4 45 44	9.72 (0.02)	8.29 (0.01)	8.01 (0.01)	7.60 (0.01)	6.80 (0.01)	4.42 (0.03)	1	1	0
5 35 28.8	-4 45 29	12.74 (0.03)	11.22 (0.01)	10.62 (0.01)	10.08 (0.02)	9.08 (0.01)	6.12 (0.01)	1	1	0
5 35 22.9	-4 45 18	12.77 (0.03)	12.31 (0.01)	12.36 (0.01)	11.96 (0.04)	10.95 (0.04)	7.08 (0.03)	0	1	0
5 36 12.4	-4 45 15		15.46 (0.08)	14.68 (0.07)	12.63 (0.09)	10.98 (0.11)	7.43 (0.06)	0	0	1

<sup>a</sup> Magnitudes from 2MASS photometry.<sup>b</sup> From Carpenter, Hillenbrand, & Skrutskie (2001); Those that are variable have Stetson indices greater than 0.55.

Table 5.: Young Stellar Object Candidates in NGC 1977 detected at 24  $\mu\text{m}$  (continued)

RA J(2000)	Dec J(2000)	$K_S^a$ mag (unc)	3.6 $\mu\text{m}$ mag (unc)	4.5 $\mu\text{m}$ mag (unc)	5.8 $\mu\text{m}$ mag (unc)	8 $\mu\text{m}$ mag (unc)	24 $\mu\text{m}$ mag (unc)	Var.	IR-ex <sup>b</sup>	Proto.
5 35 17.9	-4 44 52	10.16 (0.02)	9.59 (0.01)	9.13 (0.01)	9.16 (0.01)	8.16 (0.01)	4.84 (0.07)	1	1	0
5 35 44.5	-4 44 15	11.45 (0.02)	11.34 (0.01)	11.28 (0.01)	11.20 (0.04)	10.57 (0.08)	6.43 (0.07)	0	1	0
5 35 18.9	-4 44 10	11.91 (0.02)	11.43 (0.01)	11.25 (0.01)	10.96 (0.04)	10.28 (0.07)	7.53 (0.08)	0	1	0
5 35 33.0	-4 43 58	10.41 (0.02)	10.01 (0.01)	9.79 (0.01)	9.56 (0.01)	8.56 (0.02)	4.10 (0.05)	0	1	0
5 35 22.8	-4 43 25	12.11 (0.05)	11.62 (0.01)	11.29 (0.01)	10.85 (0.02)	9.51 (0.02)	5.71 (0.05)	1	1	0
5 35 52.3	-4 43 04	10.85 (0.02)	10.56 (0.01)	10.56 (0.01)	10.44 (0.03)	10.46 (0.05)	6.00 (0.10)	1	1	0
5 35 13.7	-4 42 58	10.64 (0.02)	10.24 (0.01)	10.01 (0.01)	9.88 (0.02)	9.22 (0.02)	6.75 (0.11)	1	1	0
5 35 42.4	-4 42 56	14.21 (0.04)	12.84 (0.03)	12.31 (0.02)	11.32 (0.05)	9.95 (0.04)	6.42 (0.02)	1	1	0
5 35 17.5	-4 42 37		12.93 (0.02)	12.27 (0.02)	11.71 (0.05)	10.93 (0.04)	8.40 (0.02)	0	1	0
5 35 22.3	-4 42 07	10.14 (0.02)	9.47 (0.01)	9.27 (0.01)	9.01 (0.01)	8.12 (0.03)	4.35 (0.07)	1	1	0
5 36 06.4	-4 41 53	10.71 (0.02)	10.30 (0.01)	10.06 (0.01)	9.64 (0.02)	8.79 (0.04)	5.41 (0.02)	0	1	0
5 35 13.2	-4 41 54	11.80 (0.02)	11.31 (0.01)	10.87 (0.01)	10.52 (0.03)	9.76 (0.03)	6.91 (0.07)	0	1	0
5 36 08.1	-4 41 20	10.71 (0.02)	10.34 (0.01)	9.95 (0.01)	9.46 (0.02)	8.63 (0.03)	5.25 (0.06)	1	1	0
5 35 25.6	-4 41 08	12.12 (0.02)	11.55 (0.01)	11.26 (0.01)	10.89 (0.04)	10.37 (0.08)	7.42 (0.03)	0	1	0
5 35 31.7	-4 41 07	12.18 (0.02)	11.85 (0.01)	11.73 (0.02)	11.63 (0.05)	11.27 (0.07)	6.10 (0.03)	1	1	0
5 35 34.5	-4 40 20	10.60 (0.02)	10.08 (0.01)	10.20 (0.01)	9.75 (0.03)	9.50 (0.10)	4.31 (0.06)	1	1	0
5 35 23.3	-4 40 10	9.53 (0.02)	7.33 (0.01)	6.25 (0.01)	5.86 (0.01)	4.66 (0.01)	1.46 (0.08)	1	0	1
5 34 52.2	-4 40 11	9.80 (0.02)	9.07 (0.01)	8.64 (0.01)	8.58 (0.01)	7.93 (0.01)	5.15 (0.06)	1	1	0
5 35 38.5	-4 38 32	12.34 (0.02)					7.63 (0.06)	1	0	0
5 35 22.8	-4 37 39						5.94 (0.27)	1	0	0

<sup>a</sup> Magnitudes from 2MASS photometry.

<sup>b</sup> From Carpenter, Hillenbrand, & Skrutskie (2001); Those that are variable have Stetson indices greater than 0.55.

## References

- Ali, B. & DePoy, D. L. 1995, *AJ*, 109, 709
- Allen, L. E., Calvet, N., D'Alessio, P., Merin, B., Hartmann, L., Megeath, S. T., Gutermuth, R. A., Muzerolle, J., Pipher, J. L., Myers, P. C., & Fazio, G. G. 2004, *ApJS*, 154, 363
- Allen, L. E., Megeath, S. T., Gutermuth, R. A., Myers, P. C., Wolk, S., Adams, F. C., Muzerolle, J., Young, E., & Pipher, J. L. 2007, in *Protostars and Planets V*, ed. B. Reipurth, D. Jewitt, & K. Keil, p. 361
- Aso, Y., Tatematsu, K., Sekimoto, Y., Nakano, T., Umemoto, T., Koyama, K., & Yamamoto, S. 2000, *ApJS*, 131, 465
- Bally, J., Langer, W. D., Stark, A. A., & Wilson, R. W. 1987, *ApJ*, 312, L45
- Baraffe, I., Chabrier, G., Allard, F., & Hauschildt, P. H. 1998, *A&A*, 337, 403
- Battinelli, P. 1991, *A&A*, 244, 69
- Brown, A. G. A. 1996, PhD thesis, Univ. of Leiden
- Brown, A. G. A., de Geus, E. J., & de Zeeuw, P. T. 1994, *A&A*, 289, 101
- Carpenter, J. M. 2000, *AJ*, 120, 3139
- Carpenter, J. M., Hillenbrand, L. A., & Skrutskie, M. F. 2001, *AJ*, 121, 3160
- Castets, A. & Langer, W. D. 1995, *A&A*, 294, 835
- Chini, R., Reipurth, B., Ward-Thompson, D., Bally, J., Nyman, L.-A., Sievers, A., & Billawalla, Y. 1997, *ApJ*, 474, L135
- Davis, C. J., Stanke, T., Froebrich, D., & Megeath, S. T. 2008, *MNRAS*, in prep.
- Dutrey, A., Duvert, G., Castets, A., Langer, W. D., Bally, J., & Wilson, R. W. 1993, *A&A*, 270, 468
- Flaherty, K. M., Pipher, J. L., Megeath, S. T., Winston, E. M., Gutermuth, R. A., Muzerolle, J., Allen, L. E., & Fazio, G. G. 2007, *ApJ*, 663, 1069
- Gatley, I., Becklin, E. E., Matthews, K., Neugebauer, G., Penston, M. V., & Scoville, N. 1974, *ApJ*, 191, L121
- Genzel, R. & Stutzki, J. 1989, *ARA&A*, 27, 41
- Goudis, C. 1982, *The Orion Complex: A Case Study of Interstellar Matter*, (Reidel, Dordrecht)
- Greene, T. P., Aspin, C., & Reipurth, B. 2008, *AJ*, 135, 1421
- Gutermuth, R. A., Megeath, S. T., Muzerolle, J., Allen, L. E., Pipher, J. L., Myers, P. C., & Fazio, G. G. 2004, *ApJS*, 154, 374
- Haro, G. 1953, *ApJ*, 117, 73
- Hillenbrand, L. A. & Hartmann, L. W. 1998, 492, 540
- Hirota, T., Bushimata, T., Choi, Y. K., Honma, M., Imai, H. et al. 2007, *PASJ*, 59, 897
- Jeffries, R. D., Maxted, P. F. L., Oliveira, J. M., & Naylor, T. 2006, *MNRAS*, 371, L6
- Jeffries, R. D. 2007, *MNRAS*, 376, 1109
- Johnson, H. M., Snow, T. P., Jr., Gehrz, R. D., & Hackwell, J. A. 1977, *PASP*, 89, 165
- Johnson, J. J., Gehrz, R. D., Jones, T. J., Hackwell, J. A., & Grasdalen, G. L. 1990, *AJ*, 100, 518
- Johnstone, D. & Bally, J. 1999, *ApJ*, 510, L49
- Jones, T. J., Mergen, J., Odewahn, S., Gehrz, R., Gatley, I., Merrill, K. M., Probst, R., & Woodward, C. 1994, *AJ*, 107, 2120
- Kirkpatrick, J. D., Reid, I. N., Liebert, J., Gizis, J. E., Burgasser, A. J., Monet, D. G., Dahn, C. C., Nelson, B., & Williams, R. J. 2000, *AJ*, 120, 447
- Kutner, M. L., Evans, N. J., & Tucker, K. D. 1976, *ApJ*, 209, 452
- Kutner, M. L., Tucker, K. D., Chin, G., & Thaddeus, P. 1977, *ApJ*, 215, 521
- Kutner, M. L., Machnik, D. E., Mead, K. N., & Evans, N. J. 1985, *ApJ*, 299, 351
- Lis, D. C., Serabyn, E., Keene, J., Dowell, C. D., Benford, D. J., Phillips, T. G., Hunter, T. R., & Wang, N. 1998, *ApJ*, 509, 299
- Luhman, K. L. 1999, *ApJ*, 525, 466
- Makinen, P., Harvey, P. M., Wilking, B. A., & Evans, N. J. 1985, *ApJ*, 299, 341
- Matthews, B. C. & Wilson, C. D. 2000, *ApJ*, 531, 868
- Megeath, S. T., Allen, L. E., Gutermuth, R. A., Pipher, J. L., Myers, P. C., Calvet, N., Hartmann, L., Muzerolle, J., & Fazio, G. G. 2004, *ApJS*, 154, 367

- Megeath, S. T., Gutermuth, R., Muzerolle, J. et al. 2008a, in prep
- Megeath, S. T., Allgaier, E., Muzerolle, J. et al. 2008b, in prep
- Menten, K. M., Reid, M. J., Forbrich, J., & Brunthaler, A. 2007, *A&A*, 474, 515
- Mezger, P. G., Wink, J. E., & Zylka, R. 1990, *A&A*, 228, 95
- Morris, M., Zuckerman, B., Turner, B. E., & Palmer, P. 1974, *ApJ*, 192, L27
- Muench, A. A., Alves, J., Lada, C. J., & Lada, E. A. 2001, *ApJ*, 558, L51
- Muzerolle, J., Megeath, S. T., Gutermuth, R. A., Allen, L. E., Pipher, J. L. et al. 2004, *ApJS*, 154, 379
- Nielbock, M., Chini, R., & Müller, S. A. H. 2003, *A&A*, 408, 245
- Ogura, K. & Walsh, J. R. 1991, *AJ*, 101, 185
- Peterson, D. E., Megeath, S. T., Luhman, K. L., Pipher, J. L., Stauffer, J. R., Barrado y Navascués, D., Wilson, J. C., Skrutskie, M. F., Nelson, M. J., & Smith, J. D. 2008, *ApJ*, in press
- Rayner, J., McLean, I., McCaughrean, M., & Aspin, C. 1989, *MNRAS*, 241, 469
- Reipurth, B. 1989, *A&A*, 220, 249
- Reipurth, B. & Aspin, C. 1997, *AJ*, 114, 2700
- Reipurth, B., Bally, J., & Devine, D. 1997, *AJ*, 114, 2708
- Reipurth, B., Rodríguez, L. F., & Chini, R. 1999, *AJ*, 118, 983
- Reipurth, B., Rodríguez, L. F., Anglada, G., & Bally, J. 2004, *AJ*, 127, 1736
- Sandstrom, K. M., Peek, J. E. G., Bower, G. C., Bolatto, A. D., & Plambeck, R. L. 2007, *ApJ*, 667, 1161
- Schwartz, R. D. 1977, *ApJS*, 35, 161
- Schwartz, R. D., Burton, M. G., & Herrmann, J. 1997, *AJ*, 114, 272
- Sharpless, S. 1959, *ApJS*, 4, 257
- Skrutskie, M. F., Cutri, R. M., Stiening, R., Weinberg, M. D., Schneider, S. et al. 2006, *AJ*, 131, 1163
- Stanke, T., McCaughrean, M. J., & Zinnecker, H. 2002, *A&A*, 392, 239 [SMZ02]
- Thronson, H. A., Harper, D. A., Keene, J., Loewenstein, R. F., Moseley, H., & Telesco, C. M. 1978, *AJ*, 83, 492
- Tsuboi, Y., Koyama, K., Hamaguchi, K., Tatematsu, K., Sekimoto, Y., Bally, J., & Reipurth, B. 2001, *ApJ*, 554, 734
- Tsujimoto, M., Koyama, K., Tsuboi, Y., Goto, M., & Kobayashi, N. 2002, *ApJ*, 566, 974
- Tsujimoto, M., Koyama, K., Kobayashi, N., Goto, M., Tsuboi, Y., & Tokunaga, A. 2003, *AJ*, 125, 1537
- Warren, W. H., Jr. & Hesser, J. E. 1978, *ApJS*, 36, 497
- Whitney, B. A., Indebetouw, R., Babler, B. L., Meade, M. R., Watson, C. et al. 2004, *ApJS*, 154, 315
- Williams, J. P., Plambeck, R. L., & Heyer, M. H. 2003, *ApJ*, 591, 1025
- Winston, E., Megeath, S. T., Wolk S. J., Muzerolle, J., Gutermuth, R., Hora, J. L., Allen, L. E., Spitzbart, B., Myers, P., & Fazio, G. G. 2007, *ApJ*, 669, 493
- Wolstencroft, R. D., Scarrott, S. M., Warren-Smith, R. F., Walker, H. J., Reipurth, B., & Savage, A. 1986, *MNRAS*, 218, 1
- Yu, K. C., Bally, J., & Devine, D. 1997, *ApJ*, 485, L45 [YBD97]
- Yu, K. C., Billawala, Y., Smith, M. D., Bally, J., & Butner, H. M. 2000, *AJ*, 120, 1974